J. Fluid Mech. (1993), *vol.* 248, *pp.* 237–265

Flow generated by a small oscillating cylinder in a mixing layer

By THOMAS F. BALSA

Department of Aerospace and Mechanical Engineering, University of Arizona, Tucson, AZ 85721, USA

(Received 7 April 1992 and in revised form 23 September 1992)

We study the flow generated by a small circular cylinder in a mixing layer. The cylinder is executing an oscillatory translation whose frequency is within the range of unstable frequencies of the shear layer. The smallness of the cylinder is measured by the ratio of its radius to the characteristic thickness of the layer. This (small) ratio serves as the expansion parameter for our theory; the flow naturally divides into inner and outer regions. The former is in the immediate vicinity of the cylinder and the latter is the far field which contains the instability waves. The solution to this problem is obtained by the method of matched asymptotic expansion. One objective is to study the dependence of this solution on various parameters such as the frequency of oscillation, velocity ratio, etc., and thus shed light on the associated *receptivity*. Other objectives deal with a restatement of causality and with the hydrodynamic field near the streamwise location of the cylinder. We find that receptivity is a strong function of frequency and velocity ratio and that the local hydrodynamic field may be quite large. Causality is restated in terms of the well-known exponential integral.

1. Introduction

The classical work on hydrodynamic instability almost exclusively focused on the determination of the dispersion relation and on the spatial structure of the instability modes in a variety of flows in which different physical effects (e.g. buoyancy, rotation, shear, etc.) were responsible for the instability (Chandrasekhar 1961; Betchov & Criminale 1967; Drazin & Reid 1981). These instability modes are always generated by a 'source', be it an oscillating ribbon, impinging acoustic waves, free-stream turbulence, or simply imperfections or vibrations of the bounding surface, among the many possibilities. Nevertheless, serious and continued attempts to establish the quantitative connection between the source of the disturbance and the instability mode are relatively recent. The subject that deals with this connection is called *receptivity*, a term coined by Morkovin, who recognized its importance about 25 years ago. The seminal analytical work is due to Goldstein (1983, 1985; see the review article by Goldstein & Hultgren 1989).

Physically speaking, we study the flow produced by a cylinder with radius much smaller than the characteristic thickness of the mixing layer. The cylinder is executing an oscillatory translation, whose frequency is in the range of unstable frequencies of the mixing layer. Thus, the present problem falls within a class of receptivity phenomena of which perhaps the best known example is the classical Schubauer–Skramstad (1943) experiment. Kerschen and his students (Heinrich, Choudhari & Kerschen 1988; Kerschen 1992, private communication) have

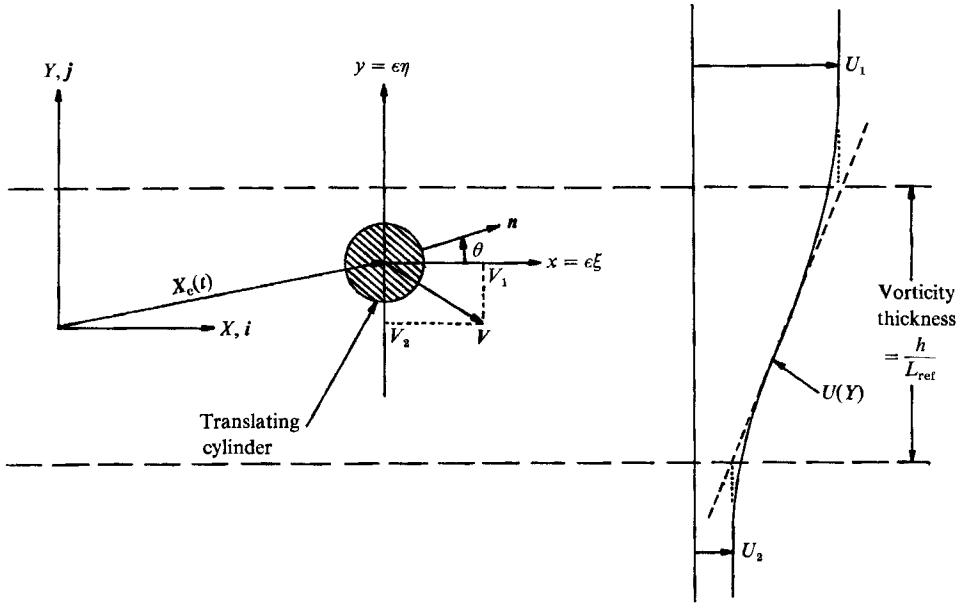

FIGURE 1. Geometry of problem (not to scale).

extensively studied several aspects of receptivity in order to understand the effects of rapid variations of wall suction/wall admittance and that of isolated surface bumps, etc., in the presence of acoustic or vorticity waves. They consider a high Reynolds number boundary layer using triple-deck theory. On the other hand, the original work of Goldstein (1983) deals with a different mechanism, which is now referred to as 'leading-edge receptivity'. The subsequent work of Goldstein (1985) does examine receptivity arising from the scattering of acoustic waves by small variations in surface geometry.

In this paper we establish a connection between the oscillatory translation of a small circular cylinder in a mixing layer and the instability wave it produces. See figure 1 for the geometry of the problem. As such, our paper addresses the issue of receptivity, but we have two other objectives as well. First, since the cylinder is small (in a sense that will be made precise shortly), the instability wave is essentially produced by point singularities in the mixing layer. Hence we derive the multipole solutions of a Rayleigh-like equation and study their near and far fields. This is done quite generally through a combination of analytical and numerical techniques in which a closed-form solution, expressed as a Fourier transform, is inverted numerically.

Second, the steady-state oscillatory solution that we obtain has to satisfy causality. This requirement leads to an examination of the original ideas of Briggs (1964) and Bers (1975) and to a restatement of these ideas in general and simple terms that is based on a discussion of the branch cuts of the well-known exponential integral. A clear criterion is presented for the selection of one of two possible branches. This ensures causality. Huerre & Monkewitz (1985, 1990) have greatly increased the awareness of causality, and the formal mathematical procedures associated with it, in the fluid mechanics community.

Since our cylinder is small, it sets up a well-identifiable inner flow in its vicinity. The relevant lengthscale for this flow is the cylinder radius. Roughly speaking, this

inner flow is equivalent to the flow around a cylinder placed in a uniform shear; such flows have been studied extensively, beginning with the work of Taylor (1917).

There is little doubt that the instability waves in mixing layers (with an inflexional velocity profile) are essentially inviscid. Through the receptivity mechanism, these waves couple with the inner flow in the vicinity of the cylinder. Obviously it is simplest to investigate this coupling if the inner flow itself is assumed to be inviscid; this is exactly what we do in this paper.

In a real fluid, the inner flow is likely to be quite complicated and certainly dependent on the Reynolds number. Thus the present solution is only a qualitative guide to what may happen in an actual fluid; direct quantitative comparisons are possible for streamlined bodies only. Work is in progress along this direction. We believe, however, that the situation is not as bad as it may appear at first sight for the following three reasons. First, any vortex shedding from the cylinder occurs at frequencies which are very much larger than the unstable frequencies of the mixing layer so that this unsteadiness of the inner flow is unimportant of our purposes (for more discussion, see (9*a*) and below). Second, for certain Reynolds numbers, the time-averaged inner flow around the cylinder forms closed streamlines and an equivalent body. It is actually the distant potential field of this latter body that couples with the instability modes in a real fluid. The entire analysis can be carried through with this generalization in mind (for more detail see §3). Finally, because the mixing layer is thick with respect to the radius of the cylinder, the instability wave is effectively produced by point-like disturbances (i.e. multipoles). A most important property of these disturbances is their quadrupole strengths; it is actually these that couple with the outer field. Thus, as long as we obtain reasonable estimates for the quadrupoles, the qualitative features of the problem will be reproduced quite well.

Let us now elaborate on the last point and introduce the outer field, which scales on the thickness of the mixing layer. On this scale, the cylinder and the inner flow have degenerated into point disturbances given by multipole solutions of the linearized Euler equations (which may be combined into a single Rayleigh-like equation for convenience).

In our model problem it is possible to relate the quadrupole strengths to the Kutta–Joukowski forces (due to the shear of the base flow) acting on the cylinder; in a sense, the outer flow may be thought of as arising from these forces acting on the fluid. However, the oscillating cylinder also experiences an apparent mass force, but it produces no disturbances in the outer region. Thus the receptivity with respect to this force is zero. Since we do not consider the drag force on the cylinder, we cannot assess its importance on the receptivity. Nevertheless, we emphasize the following: forces arising from different physical effects (e.g. Kutta–Joukowski *vs.* apparent mass) have very different influences on the outer region, and the effects of these forces (if known) may be superimposed since the flow in the outer region is governed by linear equations. We speculate that it is the Kutta–Joukowski force that couples most strongly with the instability mode since both of them originate from the shear of the base flow. If this is indeed true, then it is the Kutta–Joukowski force that determines receptivity. This aspect of the physics is reproduced quite well in our model problem. Thus the problem under consideration is indicative of what may happen in a real fluid.

To summarize, we use the method of matched asymptotic expansion to study the flow produced by a small oscillating cylinder in an (unstable) mixing layer. The inner field in the vicinity of the cylinder scales on its radius and is given by the flow around a cylinder in a uniform shear (see Lighthill 1958). The outer flow scales on the

thickness of the mixing layer; since this is large in comparison to the radius, the outer flow is essentially due to multipoles. The asymptotic matching determines the strength of the multipoles, that is, the connection between the inner and outer fields.

The outline of the paper is as follows: The formulation of the problem, together with some additional remarks, is carried out in §2. The solutions in the inner and outer regions are presented in §§3 and 4; Appendices A–C support the analyses in these sections. The asymptotic matching between the inner and outer solutions is given in §5.1, with the central result of the paper contained in (28), while the numerical inversion of the Fourier transform and causality are discussed in §5.2 and Appendix D. A discussion of results and conclusions follow in §6.

2. Formulation of problem

As discussed above, the problem under consideration deals with the *unsteady* (and to a lesser extent with the steady) flow field produced by a harmonically translating circular cylinder of very small radius in a incompressible and inviscidly unstable mixing layer. Our main objectives are to obtain the complete causal solution in the sense of Briggs and Bers (Briggs 1964; Bers 1975), to examine the receptivity of the instability mode and its dependence on various parameters, and to assess the importance of the 'hydrodynamic' field ahead of and behind the cylinder.

All variables are non-dimensional unless otherwise stated. Let $(L_{\rm ref}, U_{\rm ref})$ denote a reference length (the characteristic thickness of mixing layer) and a reference speed (the characteristic speed of mixing layer), respectively, which are used to normalize all lengths and velocities. There is no need to be more specific about these quantities. Their ratio, $L_{\rm ref}/U_{\rm ref}$, defines a transit time for the normalization of times T and t.

It turns out to be useful to use two different coordinate systems: a laboratory frame $(\boldsymbol{X}, T)$ and a frame attached to the translating cylinder, $(\boldsymbol{x}, t)$. The latter is convenient because, in it, the cylinder surface is independent of time (resulting in a simplification of boundary conditions) whereas the former is useful for specifying the unperturbed base flow and describing the instability wave. These coordinate frames are related by the transformation

$$\boldsymbol{X} = \boldsymbol{x} + \boldsymbol{X}_{\rm c}(t), \quad T = t, \tag{1a, b}$$

where $\boldsymbol{X} = \boldsymbol{X}_{\rm c}(t) = \boldsymbol{X}_{\rm c}(T)$ (or, equivalently, $\boldsymbol{x} = 0$) gives the instantaneous position of the centre of the cylinder. This position is expressed as

$$\boldsymbol{X}_{\rm c}(t) = \boldsymbol{X}_0 + \epsilon\boldsymbol{\delta}(t), \tag{1c}$$

with $\boldsymbol{X}_0 = \text{const.}$, $\boldsymbol{\delta}(t) = O(1) \sim \exp(\mathrm{i}\omega t)$, where ω is the circular frequency of oscillation and $\mathrm{i} = \sqrt{-1}$. Thus the average position of the cylinder centre in the laboratory frame is $\boldsymbol{X}_0$, and $\epsilon\boldsymbol{\delta}$ is the unsteady deviation from this point. Note that (for no special reason) the temporal oscillations take the form $\exp(\mathrm{i}\omega t)$ rather than $\exp(-\mathrm{i}\omega t)$. The latter is more customary in problems of this type.

The non-dimensional parameter, $\epsilon > 0$, is the ratio of the characteristic magnitude of the unsteady cylinder displacement and $L_{\rm ref}$; specifically, we define $\epsilon = O(a/L_{\rm ref}) = a/L_{\rm ref}$, where a is the (dimensional) radius of the cylinder. Thus the cylinder is permitted to undergo $O(1)$ displacements with respect to its radius. In typical analytical studies of receptivity, the physical size of the disturbance (producing the instability) is usually much smaller than the characteristic thickness of the shear layer. For this reason we assume that ϵ is very small so that it will serve as the perturbation parameter of our asymptotic theory. The frequency of oscillation,

$\omega = O(1)$, is chosen such that some of the instability modes of the mixing layer will be excited by the oscillating cylinder. Note that any 'intrinsic' unsteadiness associated with the flow around the cylinder (e.g. vortex shedding) has characteristic frequency $O(\epsilon^{-1}) \gg 1$. This intrinsic unsteadiness is unimportant for our purposes.

The unperturbed flow is assumed to be a transversely sheared mixing layer of an ideal fluid, whose velocity relative to the laboratory system is

$$\boldsymbol{U} = U(Y)\,\boldsymbol{i}, \tag{2a}$$

where $\boldsymbol{X} = (X, Y)$, with X along the streamwise direction and $\boldsymbol{i}$ the corresponding unit vector. The assumptions arising from the use of a parallel base flow are well known from classical stability theory; they are valid when the lengthscale associated with the spreading of the unperturbed flow (owing to viscous effects) is long in comparison to the wavelength of the disturbance. This we shall take for granted. Throughout the analysis, $U(Y)$ is an arbitrary function; for simplicity, numerical results are given for the Rayleigh piecewise linear profile (see (B 1)). The flow is assumed to be two-dimensional. The unperturbed pressure is a constant (taken to be zero without loss of generality), and pressure perturbations are normalized by $(\rho U_{\mathrm{ref}}^2)$, where $\rho = \text{const.}$ is the (dimensional) fluid density. The velocity of the cylinder relative to the laboratory system is the time derivative of $\boldsymbol{X}_c$; namely, $\epsilon\dot{\boldsymbol{\delta}}(t) = \epsilon \boldsymbol{V}(t)$, where the dot denotes differentiation with respect to the argument. Thus the speed of the cylinder is small, $O(\epsilon)$, with respect to the speed of the fluid, $O(1)$. Therefore, at lowest order in ϵ, we shall be concerned with the flow around a stationary cylinder. To be concrete, set

$$\boldsymbol{\delta}(t) = (\delta_1, \delta_2) = \mathrm{Re}\{a_1 \exp[\mathrm{i}(\omega t + \phi)], a_2 \exp(\mathrm{i}\omega t)\}, \tag{2b}$$

where $a_1 \geqslant 0$ and $a_2 > 0$ denote the amplitudes of the streamwise and cross-stream cylinder displacements, real ϕ is the arbitrary phase difference between these displacements, and $\mathrm{Re}(\cdot)$ denotes the real part of a complex number. Under these conditions, the centre of the cylinder traces out a Lissajous figure whose precise shape depends on the amplitude ratio, a_1/a_2, and the phase difference, ϕ. The frequency of motion is the same in both directions, although it is simple enough to relax this requirement. The geometry of the problem is shown in figure 1 (see also figure 11 (Appendix B) for the piecewise linear profile).

The equations of motion are continuity and Euler's equations. Let $\boldsymbol{u}$ and p be the perturbation velocity (with respect to the laboratory frame) and pressure, respectively, and define

$$\boldsymbol{v} = (u, v) = \boldsymbol{u} - \epsilon \boldsymbol{V}, \quad P = p + \epsilon \dot{\boldsymbol{V}} \cdot \boldsymbol{x}, \tag{3a, b}$$

where $\boldsymbol{V}(t) = (V_1, V_2) = \dot{\boldsymbol{\delta}}$ is the scaled translational velocity of the cylinder. Thus $\boldsymbol{v}$ denotes the perturbation velocity of the fluid relative to the cylinder and P is a pseudo-pressure that arises from non-inertial effects in the $\boldsymbol{x}$-frame attached to the cylinder. The governing equations are

$$\boldsymbol{\nabla} \cdot \boldsymbol{v} = 0, \quad \mathrm{D}\boldsymbol{v}/\mathrm{D}t + \boldsymbol{v} \cdot \boldsymbol{\nabla} \boldsymbol{v} + U' \boldsymbol{i}(\boldsymbol{v} + \epsilon \boldsymbol{V}) \cdot \boldsymbol{j} = -\boldsymbol{\nabla} P, \tag{4a, b}$$

where

$$\boldsymbol{\nabla} = \frac{\partial}{\partial \boldsymbol{x}}, \quad \frac{\mathrm{D}}{\mathrm{D}t} = \frac{\partial}{\partial t} + U \frac{\partial}{\partial x}, \tag{4c, d}$$

$U = U(Y), U' = U'(Y) = \mathrm{d}U(Y)/\mathrm{d}Y, \boldsymbol{x} = (x, y)$, and $\boldsymbol{j}$ is the unit vector in the cross-stream direction. The boundary condition on the surface of the cylinder (no relative flux) is

$$\boldsymbol{v} \cdot \boldsymbol{n} = -U \cos\theta \quad \text{on} \quad (x^2 + y^2)^{\frac{1}{2}} = \epsilon, \tag{5a}$$

where $\boldsymbol{n} = (\cos\theta, \sin\theta)$ denotes the unit outward normal to the cylinder ($\tan\theta = y/x$). Note from (1),

$$Y = y + Y_0 + \epsilon\delta_2(t), \tag{5b}$$

with $\boldsymbol{X}_0 = (X_0, Y_0) = \text{const.}$ (though, without loss of generality, we set $X_0 = 0$). Thus (4*b*) has time-varying coefficients but, in spite of this, it is convenient to use the equations in this form. The boundary condition at infinity requires that the perturbation quantities $\boldsymbol{u}$ and p vanish there. The flow is assumed to be two-dimensional.

We wish to solve (4) and (5), under the assumption that ϵ is asymptotically small; we shall use the method of matched asymptotic expansion. The solution we seek is the 'steady-state' oscillatory solution that satisfies causality.

There are two disparate lengthscales in the problem, namely the cylinder radius (non-dimensionally) $\epsilon = a/L_{\text{ref}} \ll 1$ and the vorticity thickness of the mixing layer (non-dimensionally) $h/L_{\text{ref}} = O(1)$. The inner region, the vicinity of the cylinder, is defined by $\boldsymbol{x} = O(\epsilon)$ or simply

$$\boldsymbol{\xi} = \boldsymbol{x}/\epsilon = O(1), \tag{6}$$

where $\boldsymbol{\xi} = (\xi, \eta)$ is the inner variable. The outer region is defined by $\boldsymbol{x} = O(1)$ or, more usefully, $\boldsymbol{X} = O(1)$. We shall describe the outer field in terms of $\boldsymbol{X}$ and T and the inner field in term of $\boldsymbol{\xi}$ and t. We emphasize that the governing equations are exact so far, subject to the limitations of incompressibility and negligible viscous effects. The field equations in the outer region are readily obtained from (4*a*, *b*) by setting $\boldsymbol{V}$ to zero and replacing ∇ by $\partial/\partial\boldsymbol{X}$ and t by T.

3. Inner region

The perturbation quantities in the inner region expand in powers of ϵ:

velocity $$\boldsymbol{v} = (u, v) = \boldsymbol{v}^{(0)} + \epsilon\boldsymbol{v}^{(1)} + \epsilon^2\boldsymbol{v}^{(2)} + \ldots, \tag{7a}$$

pseudo-pressure $$P = P^{(0)} + \epsilon P^{(1)} + \epsilon^2 P^{(2)} + \ldots, \tag{7b}$$

where all superscripted quantities are $O(1)$ and the ellipses stand for higher-order terms in the expansion that are not needed. The expansion of the perturbation pressure, p, is obtained from (7*b*) with p substituted for P.

The procedure for obtaining the solution is standard and there are few surprises. Therefore we shall omit most of the algebraic details. It is perhaps worthwhile to note that the boundary conditions at various orders of ϵ are obtained by substituting (5*b*) and (7*a*) into (5*a*), expanding the right-hand side in Taylor series, and collecting powers of ϵ.

The lowest-order solution is especially simple and is given by the classical result

$$\boldsymbol{v}^{(0)} = (u^{(0)}, v^{(0)}) = -(U_0/r^2)(\cos 2\theta, \sin 2\theta), \tag{8a}$$

$$P^{(0)} = p^{(0)} = \frac{U_0^2 \cos 2\theta}{r^2} - \frac{U_0^2}{2r^4}, \tag{8b}$$

where

$$r = (\xi^2 + \eta^2)^{\frac{1}{2}}, \quad \tan\theta = \eta/\xi, \quad U_0 = U(Y_0). \tag{8c–e}$$

It is not difficult to see from basic considerations that in an ideal fluid the curl of $\boldsymbol{v}^{(0)}$ must vanish so that the lowest-order flow is indeed potential at the local velocity

$U_0\boldsymbol{i}$. We call the right-hand side of (8*a*) a quadrupole field. (Note that in two-dimensional flows, there are four quadrupoles, of which only two are linearly independent).

The relevance of the potential flow around a bluff body is certainly questionable in a real fluid. Although this flow will not exist all the way to the body, it is likely to exist in the general vicinity of the body provided that the wake is closed. This is sufficient for the purposes of this paper, which deals with a model problem for a certain type of receptivity. Let us elaborate.

The actual flow around the cylinder will depend on the (cylinder) Reynolds number, which is on the order of (ϵRe), where $Re = (\rho UL/\mu)_{\text{ref}}$ is the shear-layer characteristic Reynolds number (μ is the actual viscosity). If we chose Re such that $\epsilon Re \sim O(100)$, we believe that (8*a*) (and its generalization described below) has relevance to our problem.

Under these conditions we can generally write the lowest-order velocity field as

$$\boldsymbol{v}^{(0)}(\xi, t) = \sum_{n=-\infty}^{\infty} \boldsymbol{v}_n^{(0)}(\xi) \exp(in\omega_s t), \tag{9a}$$

where $\omega_s = O(St/\epsilon) \gg 1$, $St = O(1)$ is the characteristic Strouhal number of vortex shedding and $\boldsymbol{v}_n^{(0)}$ is the nth Fourier coefficient. Equation (9*a*) represents a purely periodic time signal whose fundamental frequency, ω_s, is very much larger than the neutral frequency of the mixing layer, $\omega_N = O(1)$. Therefore, only the zeroth harmonic or the steady part, $\boldsymbol{v}_0^{(0)}(\xi)$, will play any role physically in our problem. If one specific streamline associated with $\boldsymbol{v}_0^{(0)}$ and the oncoming local stream, $U_0\boldsymbol{i}$, is closed, this streamline represents an equivalent body. Some small distance away from this equivalent body, the flow is nearly irrotational (since $Re \gg 1$) so

$$\boldsymbol{v}_0^{(0)}(\xi) = \sum_{n=2}^{\infty} \left\{ \boldsymbol{A}_n \frac{\cos n\theta}{r^n} + \boldsymbol{B}_n \frac{\sin n\theta}{r^n} \right\}, \tag{9b}$$

for suitable coefficients $\boldsymbol{A}_n = \text{const.}$ and $\boldsymbol{B}_n = \text{const.}$ Equation (9*b*) represents the general solution to Laplace's equation, which decays as $r \to \infty$. For the ideal flow around the cylinder, $\boldsymbol{A}_2 = (-U_0, 0), \boldsymbol{B}_2 = (0, -U_0)$, and $\boldsymbol{A}_n = \boldsymbol{B}_n = 0$ for $n \geqslant 3$.

Now recall transformation (1); specifically, the cylinder-fixed frame, $\boldsymbol{x}$, and the laboratory frame, $\boldsymbol{X}$, oscillate relative to each other. Therefore, even though (9*b*) is steady in the inner region, it will induce an unsteady field in the outer. At leading order, one part of the total unsteady outer field is determined by $\boldsymbol{A}_2$ and $\boldsymbol{B}_2$, since the other multipoles decay too rapidly at infinity. We remark that, in addition to this part, there are other, equally important, parts that arise from the unsteadiness (at higher orders in ϵ) in the inner region. We shall examine these shortly. Thus in order to study receptivity, we need to have characteristic values for $\boldsymbol{A}_2$ and $\boldsymbol{B}_2$; that is, we need to have the quadrupole strengths of the locally *steady* field.

Physical intuition and (8*a*) suggest that $\boldsymbol{A}_2$ and $\boldsymbol{B}_2$ should be proportional to the local speed, U_0, although generally we shall not have $\boldsymbol{A}_2 \cdot \boldsymbol{B}_2 = 0$ (which arises from the perfect symmetry of a circular cylinder). By examining the real flow in the immediate vicinity of a body and its closed wake, it is possible to relate in principle (but very difficult in practice) the two coefficients above to the actual geometry of the body. Equation (8*a*) provides one such relationship; it is simple but its connection to a real problem is qualitative. We are content with this qualitative connection since our principal goal is to provide characteristic values for receptivity and to study its variation with the parameters of the problem. In passing, we note

that the entire analysis can still be carried out if $\boldsymbol{v}^{(0)}$ (of $8a$) is replaced by $\boldsymbol{v}_0^{(0)}$ (of $9b$). In other words, the success of the theory does not depend on the simple form of ($8a$); it depends on how well we can estimate $\boldsymbol{A}_2$ and $\boldsymbol{B}_2$. Thus the present theory provides a framework for future studies along these lines. We now turn to the discussion of the unsteady inner flow at higher orders.

We assume that the unsteady flow at higher orders in the inner region, arising from the back-and-forth motion of the cylinder, is reasonably well described by inviscid flow. This might place some additional restriction on the amplitudes of motion, a_1 and a_2 of ($2b$). It is known that for an impulsively started cylinder, the flow at the rear stagnation point begins to separate when the displacement of the cylinder is about 0.35 of its radius (Batchelor 1967, p. 323). If the motion of the cylinder is reversed during this displacement, the transient process starts over again, and gross separation of the flow, accompanied by formation of wakes, is inhibited.

Since the higher-order solutions are determined by a perturbation analysis, they are governed by linear equations. Because of this, it is possible to separate these solutions into steady, $(\cdot)_{\mathrm{s}}$, and unsteady, $(\cdot)_{\mathrm{u}}$, parts

$$(\cdot) = (\cdot)_{\mathrm{s}} + (\cdot)_{\mathrm{u}}, \tag{10}$$

under the assumption $\omega \neq 0$. At $O(\epsilon)$ the perturbed flow is again irrotational; this time the oncoming local flow is a uniformly sheared flow with constant vorticity. For this reason, the vorticity equation is identically satisfied and the perturbation vorticity vanishes. Straightforward analysis shows

$$\boldsymbol{v}_{\mathrm{u}}^{(1)} = (u_{\mathrm{u}}^{(1)}, v_{\mathrm{u}}^{(1)}) = \frac{V_1 - U_0' \delta_2}{r^2}(\cos 2\theta, \sin 2\theta) + \frac{V_2}{r^2}(\sin 2\theta, -\cos 2\theta) - \boldsymbol{V}, \tag{11a}$$

where $U_0' = \mathrm{d}U(Y)/\mathrm{d}Y$ evaluated at Y_0 and $\boldsymbol{V} = (V_1, V_2) = \dot{\boldsymbol{\delta}}$. This solution (i.e. a cylinder in a uniform shear) was known to Taylor (1917). The unsteady pseudo-pressure is given by

$$-P_{\mathrm{u}}^{(1)} = -p_{\mathrm{u}}^{(1)} - \dot{\boldsymbol{V}} \cdot \boldsymbol{x} = U_0 u_{\mathrm{u}}^{(1)} + \boldsymbol{v}^{(0)} \cdot \boldsymbol{v}_{\mathrm{u}}^{(1)} + U_0' \delta_2 u^{(0)}. \tag{11b}$$

It is quite remarkable that the unsteady flow is also irrotational at $O(\epsilon^2)$, although the steady flow is not. For this reason, it is a simple matter to obtain

$$\boldsymbol{v}_{\mathrm{u}}^{(2)} = (u_{\mathrm{u}}^{(2)}, v_{\mathrm{u}}^{(2)}) = -\frac{U_0'' \delta_2^2}{2r^2}(\cos 2\theta, \sin 2\theta) - \frac{U_0'' \delta_2}{2r^3}(\sin 3\theta, -\cos 3\theta), \tag{12}$$

and the expression for $P_{\mathrm{u}}^{(2)}$ contains some thirteen terms. We shall not give it, although we will give expressions for both the unsteady and steady forces acting on the circular cylinder. Note that $\boldsymbol{v}_{\mathrm{u}}^{(2)}$ is identically zero if the centre of the cylinder is placed at the inflexion point of the mixing layer. In this case, the local velocity profile is exceptionally well represented by a constant shear profile so that the correction at $O(\epsilon^2)$ is absent.

In order to obtain the steady and unsteady forces, we must have the steady solutions as well. These are given for completeness in Appendix A. The steady and unsteady forces (per unit span), normalized by $(\rho U^2 L)_{\mathrm{ref}}$, are

$$\boldsymbol{F}_{\mathrm{s}} = 2\pi\epsilon^2 U_0 U_0'(0, 1) + \ldots, \tag{13a}$$

$$\boldsymbol{F}_{\mathrm{u}} = \pi\epsilon^3 \{2U_0' V_2 - \dot{V}_1, 2U_0'(U_0' \delta_2 - V_1) - \dot{V}_2 + \tfrac{3}{2} U_0 U_0'' \delta_2\} + \ldots. \tag{13b}$$

The physical origins of these forces are apparent mass effects (proportional to acceleration, $\dot{\boldsymbol{V}}$) and Kutta–Joukowski effects (proportional to shear, U_0'; interpret

$U_0'' \delta_2$ as a change in U_0' due to cylinder displacement) arising from the circulation around the cylinder created by the transversely sheared base flow. Equations (13*a*, *b*) are in complete agreement with Taylor (1917) with the exception of the U_0'' term, which he did not consider. Our purpose in giving these forces is to show later the extent to which they generate the outer field and the instability wave.

In essence, the solution in the inner region is given by the flow around a cylinder in a uniform shear (with some minor corrections for U_0''); this solution is well known (see, for example, Batchelor 1967, p. 542). For this reason, our analytical treatment has been very brief.

4. Outer region

It is convenient to describe the perturbed flow in the outer region in terms of laboratory coordinates, (X, T); in this region, $X = O(1)$. Recall that the lowest-order velocity components in the inner region decay as r^{-2} for r large. Since for large ξ (essentially large r), $\xi = O(X/\epsilon)$, the perturbation velocity and pressure in the outer region expand as:

velocity $$\boldsymbol{u} = \hat{\boldsymbol{u}} = (\hat{u}, \hat{v}) = \epsilon^2(\hat{\boldsymbol{u}}^{(0)} + \epsilon\hat{\boldsymbol{u}}^{(1)} + \dots), \tag{14a}$$

pressure $$p = \hat{p} = \epsilon^2(\hat{p}^{(0)} + \epsilon\hat{p}^{(1)} + \dots), \tag{14b}$$

where all superscripted quantities are $O(1)$ and the hat indicates that a quantity is written for the outer region. Clearly, both $(\cdot)^{(0)}$ and $(\cdot)^{(1)}$ are governed by linearized homogeneous equations since quadratic nonlinearities are no greater than $O(\epsilon^4)$. From continuity and the Euler equations, it is a simple matter to establish that $\hat{v}^{(0)}$ and $\hat{v}^{(1)}$ obey a Rayleigh-like equation

$$\mathscr{L}(v) = \frac{\mathrm{D}}{\mathrm{D}T}\nabla^2 v - U''\frac{\partial v}{\partial X} = 0, \tag{15a}$$

$$\frac{\mathrm{D}}{\mathrm{D}T} = \frac{\partial}{\partial T} + U\frac{\partial}{\partial X}, \tag{15b}$$

where v stands for $\hat{v}^{(j)}$ $(j = 0, 1)$, $U = U(Y)$, $U' = \mathrm{d}U(Y)/\mathrm{d}Y$, and $\nabla^2 = \partial^2/\partial X^2 + \partial^2/\partial Y^2$ is the Laplacian operator. The streamwise velocity component, $\hat{u}$, may be recovered from continuity and the pressure, $\hat{p}$, from either of the two momentum equations.

In order to induce a flow in the outer region, that is, to conveniently represent the effect of the translating cylinder on the outer flow, we add a combination of delta functions to the right-hand side of (15*a*). Since the unsteadiness in the inner region and the relative motion of the two coordinate frames are proportional to $\exp(\mathrm{i}\omega T)$, we write

$$\mathscr{L}(G_{nm}) = \frac{\mathrm{D}}{\mathrm{D}T}\{\exp(\mathrm{i}\omega T)(-1)^m \delta^{(n)}(X)\delta^{(m)}(Y - Y_0)\}, \tag{16}$$

for $n, m = 0, 1, 2, \dots$. The $\mathscr{L}$ on the left-hand side of (16) is the Rayleigh-like operator defined by (15*a*) and $\delta^{(n)}(\cdot)$ denotes the nth derivative of the Dirac delta function. It is understood that only the real part of G_{nm} is relevant to our problem (see (2*b*)).

The complex quantities G_{nm} may be interpreted as multipole solutions of Rayleigh's equation, corresponding to the usual multipoles of classical potential theory associated with Laplace's equation. The convective derivative, $\mathrm{D}/\mathrm{D}T$, on the right-hand side of (16) is included in order to make this correspondence as close as

possible. G_{nm} vanish as $(X^2+Y^2)^{\frac{1}{2}} \to \infty$ for $(n+m) \geqslant 1$; G_{00} behaves as $\log (X^2+Y^2)^{\frac{1}{2}}$. The outer solution is written as a suitable linear combination of G_{nm}; the coefficients in this combination are determined by asymptotic matching.

In passing we note that $\hat{\boldsymbol{u}}^{(0)}$ and $\hat{p}^{(0)}$ are independent of time; these quantities may be obtained formally from (16) by letting $\omega \to 0$. However, since our main interest is in the unsteady outer field, we shall focus our attention on $\hat{\boldsymbol{u}}^{(1)}$ and $\hat{p}^{(1)}$ only. Thus the unsteady field, hence receptivity, scales as ϵ^3 (although there is a much larger, namely $O(\epsilon^2)$, steady flow present in the outer region).

Let

$$G = G(X, Y, \omega; Y_0) = \exp(-\mathrm{i}\omega T)\, G_{00}, \tag{17a}$$

so that

$$G_{nm} = \exp(\mathrm{i}\omega T) \frac{\partial^{n+m}}{\partial X^n \partial Y_0^m} G, \quad n, m = 0, 1, 2, \ldots. \tag{17b}$$

We call G the source solution or Green's function; it is independent of time. The validity of (17*b*) is clear from differentiating the equation for G_{00} with respect to the variables indicated in (17*b*).

In order to obtain the source solution, G, hence G_{nm}, we use Fourier transform in X. Define transform pairs $[(\cdot), (\tilde{\cdot})]$ via

$$(\tilde{\cdot}) = \int_{-\infty}^{\infty} (\cdot) \exp(-\mathrm{i}kX)\, \mathrm{d}X, \quad (\cdot) = \frac{1}{2\pi} \int_{-\infty}^{\infty} (\tilde{\cdot}) \exp(+\mathrm{i}kX)\, \mathrm{d}k, \tag{18a, b}$$

where the tilde denotes the actual transform of a function of X, and k is the transform variable, which is interpreted as the streamwise wavenumber. From (16) and (18) we find

$$\left(\frac{\mathrm{d}^2}{\mathrm{d}Y^2} - k^2 - \frac{kU''}{\omega + kU} \right) \tilde{G} = \delta(Y - Y_0), \tag{19}$$

where $\tilde{G} = \tilde{G}(k, Y, \omega; Y_0)$. We recognize (19) as an inhomogeneous Rayleigh equation.

The formal solution of (19) is well known. Let $\mathscr{G}_j = \mathscr{G}_j(k, Y, \omega)$ $(j = 1, 2)$ be solutions of the homogeneous version of (19) that are proportional to $\exp(\mp \kappa Y)$ and $Y \to \pm\infty$. Here,

$$\kappa = (k^2)^{\frac{1}{2}}, \tag{20}$$

such that $\mathrm{Re}(\kappa) > 0$; when k is real, $\kappa = |k|$. In practice, the Fourier inversion, (18*b*), is accomplished by a contour deformation in the complex k-plane. Equation (20) defines κ for any value of k such that there are two branch cuts, emanating from $k = 0$, along the positive and negative imaginary axes. A small 'hole' at the origin enables us to carry out the inversion from minus to plus infinity. Making use of homogeneous solutions $\mathscr{G}_1$ and $\mathscr{G}_2$, and the usual jump conditions for $\tilde{G}$ across $Y = Y_0$, we find

$$\tilde{G} = \begin{cases} \dfrac{\mathscr{G}_1(Y)\, \mathscr{G}_2(Y_0)}{W(k, \omega)}, & Y > Y_0, \qquad (21a) \\[2ex] \dfrac{\mathscr{G}_2(Y)\, \mathscr{G}_1(Y_0)}{W(k, \omega)}, & Y < Y_0, \qquad (21b) \end{cases}$$

where, for simplicity of notation, we have suppressed the dependence of $\mathscr{G}_j$ $(j = 1, 2)$ on k and ω and

$$W = W(k, \omega) = (\mathscr{G}_1' \mathscr{G}_2 - \mathscr{G}_1 \mathscr{G}_2')_{Y = Y_0}, \tag{21c}$$

with a prime denoting differentiation with respect to Y.

Note that the Wronskian, $W(k,\omega)$, is independent of Y_0, a fact that is easy to establish from (19). This is important physically since the dispersion relation $W=0$ (or equivalently $k=k(\omega)$) is, therefore, independent of the location of the cylinder. Thus we may find the dispersion relation without any reference to the presence of the cylinder.

For a given velocity profile, $U=U(Y)$, we can solve the homogeneous version of (19) numerically in order to obtain $\mathscr{G}_j(Y)$ $(j=1,2)$ for each value of k (ω is assumed to be fixed). From (21) we find $\tilde{G}$, and numerical inversion of the Fourier transform, (18*b*), provides the Green function, G. This is not at all an impossible task, although in the present paper we opt for a simpler procedure. This consists of finding closed-form solutions for $\mathscr{G}_j(Y)$ $(j=1,2)$ using the piecewise linear profile of Rayleigh but still inverting the Fourier transform numerically. Some details about obtaining $\tilde{G}$ are provided in Appendix B.

With the construction of Green's function out of the way,

$$G=\frac{1}{2\pi}\int_{-\infty}^{\infty}\tilde{G}(k,Y,\omega;Y_0)\exp(+\mathrm{i}kX)\,\mathrm{d}k, \tag{22}$$

we can now begin the examination of G_{nm} $(n,m=0,1,2,\dots)$ for small values of X and $(Y-Y_0)$. This information is needed in order to carry out the asymptotic matching with the inner solution.

Intuitively it is clear that

$$G\sim\frac{1}{2\pi}\log R+\dots \quad \text{as} \quad R\to 0, \tag{23a}$$

where

$$R=[X^2+(Y-Y_0)^2]^{\frac{1}{2}}. \tag{23b}$$

In other words, in the immediate vicinity of the source, the term $U''\,\partial G/\partial X$ (see (15) and (16)) is negligible with respect to $\mathrm{D}/\mathrm{D}T(\nabla^2 G)$ since the latter involves higher-order derivatives that are more singular at $R\approx 0$ than those of the former.

It is possible to find analytically the behaviour of (22) as $R\to 0$ by establishing the behaviour of $\tilde{G}$ as $k\to\infty$. This may be done by solving (19) by the WKBJ method; indeed, the leading-order term from this procedure is in perfect agreement with (23*a*). There are several ways to find the corrections to (23*a*). We use a perturbation procedure in which we write

$$G=\frac{1}{2\pi}\log R+g, \tag{24a}$$

and solve the resultant equation for g at small values of R. The final expression is

$$g=\frac{U_0''}{8\pi U_0}R^2(\log R-1)+\{1,X,Y,X^2-Y^2,XY\}+O(R^3), \tag{24b}$$

where the notation $\{\dots\}$ means that g may contain an arbitrary linear combination of the entries in the braces. Fortunately, for the purposes of this paper, we do not need to know more about this combination because it is not singular at $R=0$. G_{nm} can be obtained by successively differentiating G as indicated in (17*b*). The results are tabulated in Appendix C.

5. Asymptotic matching and causality

5.1. *Matching*

The asymptotic matching is carried out for the cross-stream velocity component using the matching principle of Van Dyke (1975, p. 64) in the form '2 outer (3 inner) = 3 inner (2 outer)'. Let v_s and v_u denote the steady and unsteady components of the cross-stream velocity with respect to the laboratory reference frame. From (8a), (11a), (12), and Appendix A, we find the 3-term inner solution to be the sum of v_s and v_u where

$$v_s = -\frac{U_0 \sin 2\theta}{r^2} + \frac{\epsilon U_0'}{2r^3}\cos 3\theta + \frac{\epsilon^2 U_0''}{4}\left(\sin 2\theta - \frac{\sin 2\theta}{2r^2} + \frac{\sin 4\theta}{2r^4}\right), \tag{25a}$$

$$v_u = \epsilon\frac{V_1 - U_0'\delta_2}{r^2}\sin 2\theta - \epsilon\frac{V_2\cos 2\theta}{r^2} - \epsilon^2\frac{U_0''\delta_2^2}{2}\frac{\sin 2\theta}{r^2} + \epsilon^2\frac{U_0''\delta_2}{2}\frac{\cos 3\theta}{r^3}. \tag{25b}$$

Coordinate transformations (1a) and (6) (recall $\xi = r\cos\theta, \eta = r\sin\theta$) immediately yield the 2-term outer expansion of $(v_s + v_u)$ as

$$-2\pi\epsilon^2 U_0\left(\frac{\sin 2\Theta}{2\pi R^2} - \frac{U_0''\sin 2\Theta}{8\pi U_0}\right) + 2\pi\epsilon^3\,\mathrm{Re}\exp(\mathrm{i}\omega t)\left\{[\mathrm{i}\omega a_1\exp(\mathrm{i}\phi) - U_0' a_2]\frac{\sin 2\Theta}{2\pi R^2}\right.$$
$$-\mathrm{i}\omega a_2\frac{\cos 2\Theta}{2\pi R^2} + a_1\exp(\mathrm{i}\phi)\,U_0\left(-\frac{\sin 3\Theta}{\pi R^3} + \frac{U_0''}{4\pi U_0 R}\sin\Theta\cos 2\Theta\right)$$
$$\left. - a_2 U_0\left(-\frac{\cos 3\Theta}{\pi R^3} + \frac{U_0''}{4\pi U_0 R}\cos\Theta\cos 2\Theta\right)\right\}, \tag{26}$$

where we have eliminated the velocity, $V = (V_1, V_2)$, of the translating cylinder through the time derivative of the displacement, (2b). Note that

$$R = [X^2 + (Y - Y_0)^2]^{\frac{1}{2}}, \quad \Theta = \tan^{-1}(Y - Y_0)/X. \tag{27a, b}$$

We are now ready to match with the outer solution.

The first term in (26) is essentially a steady field; it is generated by a G_{11} quadrupole [of strength $(-2\pi\epsilon^2 U_0)$] in the limit as $\omega \to 0$. This result comes from (C 1c); the arbitrary constant in this equation is required to vanish because of matching. Thus the (XY) term in g (see (24b)) is actually absent. We shall not say more about the steady solution for the velocity.

The second term in (26) represents the unsteadiness in the outer region. The corresponding outer solution is written as a linear combination of quadrupoles and octopoles. Using the results of Appendix C, we see by inspection (or by a systematic procedure) that this combination is

$$\hat{v} = 2\pi\epsilon^3\,\mathrm{Re}\{[\mathrm{i}\omega a_1\exp(\mathrm{i}\phi) - U_0' a_2]\,G_{11} + \mathrm{i}\omega a_2 G_{20} + a_1\exp(\mathrm{i}\phi)\,U_0 G_{21}$$
$$- a_2 U_0 G_{12} + \mathrm{const.}\,(G_{20} + G_{02})\}. \tag{28}$$

In other words, (28) gives the unsteady, outer, cross-stream velocity component. Continuity immediately provides the streamwise velocity $\hat{u}$. Observe that $\hat{v}$ and $\hat{u}$ scale as ϵ^3 and depend explicitly on the frequency (ω), amplitudes (a_1 and a_2), and phase (ϕ) of the cylinder motion (see (2b)). We shall study the dependence of these velocity components on the aforementioned parameters, as well as on others such as the cylinder location, Y_0, and the velocity difference, $\Delta U = U_1 - U_2 > 0$. Recall that $\epsilon = a/L_{\mathrm{ref}} \ll 1$, where a is the (dimensional) cylinder radius, L_{ref} is the characteristic

thickness of the mixing layer, and U_0, U_0', etc., stand for U, $\mathrm{d}U/\mathrm{d}Y$, etc., evaluated at the average cross-stream location of the cylinder (at $Y = Y_0$). Equation (28) is the central result of this paper.

A most striking feature of (28) is its arbitrariness as implied by the appearance of an undetermined 'const.' This arbitrariness completely disappears for the Rayleigh piecewise linear profile since $G_{20}+G_{02} = 0$ (identically!), and is likely to be unimportant for a general velocity profile whenever the cylinder is placed at the inflexion point since $G_{20}+G_{02} \approx 0$. These observations may be derived from Appendices B and C, respectively. In order to obtain the 'const.' in (28) (i.e. essentially the relative balance between the G_{20} and G_{02} quadrupoles), the perturbation solution and the matching must be carried out to higher orders in the general case. This is a formidable task and the usefulness of the Rayleigh piecewise linear profile is apparent once more. Note that this type of arbitrariness is also absent in classical potential theory (i.e. Laplace's equation) because $G_{20}+G_{02} = 0$.

It is interesting to inquire about the dependence of the outer velocity field, $\hat{v}$, on the unsteady force acting on the cylinder. We do this for the Rayleigh piecewise linear velocity profile. Thus the non-uniqueness in (28) disappears and $U'' = 0$. After eliminating the cylinder velocity V in favour of displacements, we recast the force (13*b*) as

$$\boldsymbol{F}_{\mathrm{u}} = \mathrm{Re}\,[\exp(\mathrm{i}\omega t)\,\mathscr{F}_{\mathrm{u}}], \tag{29a}$$

where

$$\mathscr{F}_{\mathrm{u}} = 2\pi\epsilon^3 U_0' \left\{ \mathrm{i}\omega a_2 + \frac{a_1\,\omega^2 \exp(\mathrm{i}\phi)}{2U_0'}, -[\mathrm{i}\omega a_1 \exp(\mathrm{i}\phi) - U_0' a_2] + \frac{a_2\,\omega^2}{2U_0'} \right\}. \tag{29b}$$

The forces due to apparent mass effect (i.e. terms proportional to ω^2) do not induce an outer field; the y-component of the Kutta–Joukowski force induces a (1, 1) quadrupole whose strength is proportional to this force divided by $(-U_0')$, whereas the x-component induces a $(2, 0) = -(0, 2)$ quadrupole whose strength is in the same proportion (but without the minus sign). These considerations account for the first two terms on the right-hand side of (28).

The remaining two terms arise from the *steady* force, owing to the fact that the point of application of this force varies as the cylinder oscillates. Based on the remarks above and (13*a*), the steady force is expected to induce a (1, 1) quadrupole of strength $(-2\pi\epsilon^2 U_0)$ and the corresponding unsteady field is proportional to

$$-2\pi\epsilon^2 U_0 \left\{ -\epsilon a_1 \exp(\mathrm{i}\phi) \frac{\partial G_{11}}{\partial X} + \epsilon a_2 \frac{\partial G_{11}}{\partial Y_0} \right\} \tag{29c}$$

due to the small displacement of this quadrupole as a result of cylinder motion. This is in perfect agreement with (28). In summary, the lowest-order outer velocity field arises from the Kutta–Joukowski forces (steady and unsteady) acting on the cylinder.

5.2. *Causality*

In some ways the most tedious and perhaps trickiest part of our analysis is the efficient numerical inversion of the Fourier transform, (22), while maintaining causality in the sense of Briggs and Bers (Briggs 1964; Bers 1975). In order to do this, we first consider the frequency of oscillation to be complex, $\omega = \omega_{\mathrm{R}} + \mathrm{i}\omega_{\mathrm{I}}$, with $(-\omega_{\mathrm{I}})$ sufficiently large and positive. (Recall that our temporal factor is $\exp(\mathrm{i}\omega t)$ rather than $\exp(-\mathrm{i}\omega t)$.) Once the behaviour of the Fourier inversion is understood, ω_{I} will be allowed to approach zero in such a way that the analytic behaviour of the integral

(as a function of ω) is not destroyed. In this respect, the Rayleigh piecewise linear velocity profile is indispensable since it provides simple and explicit information on the behaviour of $\tilde{G}$ in the entire complex k-plane (see (B 4)).

First we separate (B 4) into four terms according to the obvious delineation provided by the four coefficients of $\exp[\pm\kappa(Y\pm Y_0)]$ for every possible combination of the $\pm$signs. Then split the Fourier integral into

$$\int_{-\infty}^{+\infty} = \int_{-\infty}^{0} + \int_{0}^{+\infty}, \tag{30}$$

so that we now have eight integrals. Each integrand is analytic in its respective half-plane ($\mathrm{Re}(k) \gtrless 0$) except for possible poles arising from the vanishing of the common factor $[(\omega-\Omega_1)(\omega-\Omega_2)]$; the singularity at $k=0$ is removed by considering only quadrupoles and octopoles. For these, the derivatives in (17*b*) 'bring down' factors of k in (B 4). From Appendix B

$$\Omega_{1,2}(k) = -kU_{\mathrm{m}} \pm \mathrm{i}\Delta U\lambda(k), \tag{31a}$$

$$\lambda(k) = \tfrac{1}{4}[\exp(-4\kappa)-(1-2\kappa)^2]^{\frac{1}{2}}, \tag{31b}$$

where $U_{\mathrm{m}} = \frac{1}{2}(U_1+U_2)$ and $\Delta U = U_1-U_2 > 0$. $\lambda(k)$ has branch-point singularities at $k = \pm k_{\mathrm{N}}$ ($k_{\mathrm{N}} \approx 0.6392$) and its branch cuts are chosen to lie along the real k-axis with $|k| > k_{\mathrm{N}}$. The neutral frequency is $\omega_{\mathrm{N}} = -k_{\mathrm{N}}U_{\mathrm{m}}$. Thus the unstable and stable dispersion relations are given by $\omega = \Omega_{2,1}(k)$, and k may be considered complex. It is important to realize that in spite of the branch cuts of $\lambda(k)$, each of the eight integrands above is analytic except for (possible) isolated poles. Thus the Fourier inversion may be evaluated along the real axis or very slightly above or below it. The choice is dictated by other considerations (see below) and generally will be different for each of the eight integrals.

Now in each of these integrals employ the partial fraction decomposition

$$\frac{1}{(\omega-\Omega_1)(\omega-\Omega_2)} = \frac{1}{\Omega_1-\Omega_2}\left(\frac{1}{\omega-\Omega_1}-\frac{1}{\omega-\Omega_2}\right), \tag{32}$$

and further subdivide each integral into two terms as suggested by (32). For example, a typical integral, $I^{(m)}$, is written as

$$I^{(m)} = I_1^{(m)} + I_2^{(m)}, \quad m = 1,\ldots,8, \tag{33}$$

where the integrand of $I_j^{(m)}$ contains the factor $[(\Omega_1-\Omega_2)(\omega-\Omega_j)]^{-1}$ ($j=1,2$). To be specific, let

$$I_1^{(1)} = \frac{1}{2\pi}\int_0^{\infty} \frac{f(k)\exp[\mathrm{i}kX-\kappa(Y-Y_0)]}{\omega-\Omega_1(k)}\,\mathrm{d}k, \tag{34a}$$

where

$$f(k) = \frac{\kappa\omega_1\omega_2+(\frac{1}{2}\Delta U)^2(\kappa-\frac{1}{4})}{\frac{1}{2}\Omega_1(k)-\Omega_2(k)} \tag{34b}$$

and $(Y-Y_0) > 0$. For $(Y_0-Y) > 0$, interchange Y and Y_0 (see Appendix B). Thus $I_1^{(1)}$ comes from the first terms of (B 4) and (32), and from the second term of (30). Note that $I_1^{(1)}$ is a contribution to G_{20} and for this reason the integrand has been multiplied by $(\mathrm{i}k)^2 = -k^2 = -\kappa^2$. Refer to (B 2*e*) for the definitions of ω_j ($j=1,2$). For the actual evaluation of the integrals, we confine our attention to (34). All other integrals may be handled in a similar manner.

Suppose that for each complex ω, with $-\mathrm{Im}(\omega) \gg 1$, $(\omega - \Omega_1(k))$ has a simple zero at $k_1^* = k_1^*(\omega)$ in the right-half of the complex plane (in other words, $\omega = \Omega_1(k_1^*)$). This supposition may be false, in which case the following arguments directly apply to (34*a*). When the supposition is true, write (34*a*) as

$$I_1^{(1)} = \frac{1}{2\pi}\int_0^\infty F(k)\exp\left[ikX - \kappa(Y-Y_0)\right]\mathrm{d}k$$

$$-\frac{1}{2\pi}\frac{f(k_1^*)}{\Omega_1'(k_1^*)}\int_0^\infty \frac{\exp\left[ikX-\kappa(Y-Y_0)\right]}{k-k_1^*}\mathrm{d}k, \quad (Y-Y_0) > 0, \quad (35a)$$

$$F(k) = \frac{f(k)}{\omega - \Omega_1(k)} + \frac{f(k_1^*)}{\Omega_1'(k_1^*)(k-k_1^*)}, \quad (35b)$$

where $\Omega_1' = \mathrm{d}\Omega_1/\mathrm{d}k \neq 0$. In essence, we have subtracted out the 'singularity' at the pole in the first term and added it back in the second term of (35*a*).

In order to evaluate the first integral in (35*a*), deform the contour from the immediate vicinity of the real axis to the ray

$$k_\mathrm{I} = \frac{X}{Y-Y_0}k_\mathrm{R}, \quad k_\mathrm{R} \geqslant 0, \quad (36)$$

where $k = k_\mathrm{R} + ik_\mathrm{I}$. If $X/(Y-Y_0)$ is positive (negative), the ray is in the first (fourth) quadrant. In order to accomplish this contour deformation without any additional consideration for the presence of the branch cut, choose the original path of the Fourier inversion to lie slightly above (below) the real axis in the right-half plane. This can always be done since the branch cuts of Ω_j $(j = 1, 2)$ play no role in Fourier inverse, (22), as explained near the end of Appendix B. The point is that $F(k)$ is analytic (except for the branch cut along $k > k_\mathrm{N}$) so that no singularities are crossed during this contour deformation. There is no difficulty in closing the contour at infinity.

Along this ray, the first integral of (35*a*) is of Laplace type. The integrand decays exponentially along the ray, and the integral may be evaluated with extreme efficiency and accuracy using Laguerre integration (essentially a Gauss quadrature; Abramowitz & Stegun 1970, p. 923). Typically, we use either 5- or 15-point integration, compare corresponding results, and find that they always agree to many significant figures. There is also no difficulty in letting $\mathrm{Im}(\omega)$ approach zero in the first integral.

Evidently the issue of causality is entirely contained in the second integral of (35*a*). This is nothing more than the exponential integral, and causality is intimately related to choosing the correct branch cuts (in complex ω-space) for this integral. This is done in Appendix D. The numerical evaluation of the exponential integral is accomplished through its known Taylor and asymptotic series representation (Abramowitz & Stegun 1970, pp. 229, 231).

There are two points worth noting. First, in many theoretical studies, it is suggested that Fourier inverse, (22), may be evaluated by closing the contour at infinity and picking up the contributions from the residues and branch cuts. Although this is certainly true, the procedure does not provide a numerically efficient method; initial trials along these directions revealed that even with 10000 points along the cut (and not separating the integral into various parts), the accuracy of the integral could not be guaranteed for all values of the parameters and X and Y. Second, M. Gaster (1992, private communication) in his recent studies has also inverted

Fourier transforms numerically. This procedure might be called 'multiplicative', while ours is 'additive'. With reference to (34*a*), Gaster multiplies and divides the integrand by $(k-k_1^*)$ in order to produce two factors, one that is analytic and another that is singular and behaves as $(k-k_1^*)^{-1}$. The analytic part is inverted numerically along the real axis while the singular part is inverted in closed form. The value of the Fourier inverse is determined from the convolution theorem and the aforementioned results. Gaster also satisfies causality.

We repeat (and emphasize) that the closing of the contour at infinity is correct in principle. Since there are branch cuts along the imaginary axes (see (20)), such a contour deformation of the Fourier inverse not only picks up the sum of the residues at the poles but also the integrals along the branch cuts. The corresponding integrands have an oscillatory behaviour; therefore, the numerical evaluation of the integrals is not entirely without difficulty. The situation is further aggravated by the fact that for certain (complex) ω, the roots of the dispersion relation actually run into the branch cut; for these ω, enormous care must be exercised to obtain accurate values of the integral. To be sure, in this case the branch cut itself may be moved, but we feel that in order to avoid unnecessary complexity in the computer code, the proposed method is the cleanest. Its accuracy is superb, with very few nodes required for the integration.

6. Discussion and conclusions

In order to calculate the complete velocity field in the outer region, we use (28), in which the quadrupole solutions, G_{nm}, are determined from a numerical inversion of their Fourier transforms. To study receptivity and to examine the role of the instability mode downstream of the cylinder, we also provide an approximate evaluation for (28). The discussion is restricted to the Rayleigh piecewise linear profile for simplicity.

Suppose ω is the (real) frequency of oscillation and $k_0 = k_0(\omega)$ is the corresponding unstable spatial eigenvalue. We write

$$G_{nm} \approx \frac{1}{2\pi}\exp\left[\mathrm{i}(\omega T + k_0 X)\right] R_{nm}, \quad n, m = 0, 1, 2, \ldots, \tag{37a}$$

where $(R_{nm}/2\pi\mathrm{i})$ (independent of time but dependent on Y) is the residue of $\tilde{G}_{nm}\exp(-\mathrm{i}\omega T)$ at the unstable pole (see (22)). Thus, from (28) and the residue theorem,

$$\hat{v} \approx \epsilon^3 a_2 \,\mathrm{Re}\{\exp\left[\mathrm{i}(\omega T + k_0 X)\right] \mathscr{R}_v\}, \tag{37b}$$

where

$$\mathscr{R}_v = \left\{\left(\frac{\mathrm{i}\omega a_1}{a_2}\exp(\mathrm{i}\phi) - U_0'\right) R_{11} + \mathrm{i}\omega R_{20} + \frac{a_1 U_0}{a_2}\exp(\mathrm{i}\phi) R_{21} - U_0 R_{12}\right\}, \quad a_2 > 0. \tag{37c}$$

Clearly (37*b*) is a good approximation far downstream ($X \gg 1$) where the instability wave dominates because of its exponentially increasing character as measured by $[\mathrm{Im}\,(k_0)]$.

The receptivity (of the v-velocity) is measured by $|\mathscr{R}_v|$ in the following sense. Let $\hat{v}_{\mathrm{m}}^2$ denote the mean-square average of $\hat{v}$ over one cycle of oscillation. Thus

$$\hat{v}_{\mathrm{m}} = \frac{\epsilon^3 a_2}{\sqrt{2}}\exp\left[-\mathrm{Im}\,(k_0) X\right] |\mathscr{R}_v| \tag{38}$$

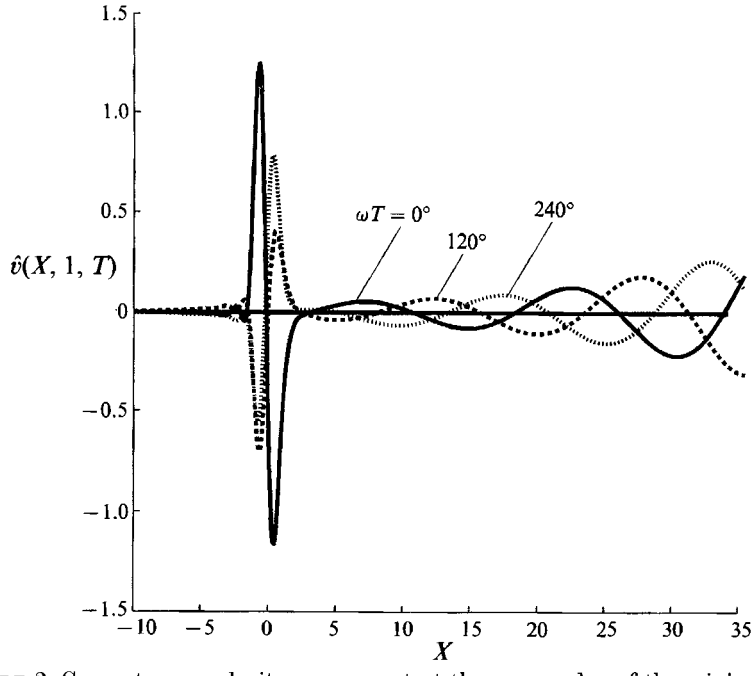

FIGURE 2. Cross-stream velocity component at the upper edge of the mixing layer, for three values of time: $U_1 = 1, U_2 = 0.5, \omega = 0.3, a_1/a_2 = 0, Y_0 = 0$.

and the maximum of $|\mathscr{R}_v|$ over Y ($-1 \leqslant Y \leqslant 1$), for fixed parameters such as a_1/a_2, ϕ, Y_0, ω, ΔU, etc., is defined to be the receptivity of the v-velocity (in 'units' of $\epsilon^3 a_2/\sqrt{2}$). An entirely analogous quantity measures the receptivity of the u-velocity, say $|\mathscr{R}_u|$. These two receptivities will have different numerical values. In other words, receptivity is defined to be directly proportional to the maximum value of the 'intensity' associated with a fluctuating quantity in the mixing layer proper.

In order to get some feel for the nature of the flow field, we show in figures 2–5 $\hat{v}(X, Y, T)$ (measured in units of $\epsilon^3 a_2$) as a function of X for three values of time: $\omega T = 0°$, 120°, and 240°. The field point is located at the upper edge of the mixing layer, $Y = 1$. The precise values of the various parameters are indicated in the individual figures.

In figure 2 we show the complete cross-stream velocity component as obtained from the numerical inversion of the Fourier transform. It is characterized by: (i) a rapidly decaying (the decay is algebraic in X) 'hydrodynamic' field ahead of the cylinder (located at $X = 0$), (ii) a large 'local' field in the vicinity of $X = 0$ which spans the entire mixing layer, and (iii) a wave-like disturbance behind the cylinder (roughly the instability wave) which grows in amplitude with distance downstream. The three successive time traces show very nicely the convected character of this wave.

It is important to realize that the large local field in the vicinity of $X = 0$ does not arise from the fact that the field point is close to the location of the cylinder; in fact, these points are well separated in this example since $Y_0 = 0$ and $Y = 1$ (and, of course, $\epsilon \ll 1$). To be sure, as $(Y - Y_0)$ is reduced (increased), the peak of the local field increases (decreases), but the fact that a strong local field is present across the entire mixing layer is quite remarkable. Similar results have been observed by M. Gaster (1992, private communication) in his recent wall-boundary layer studies. As

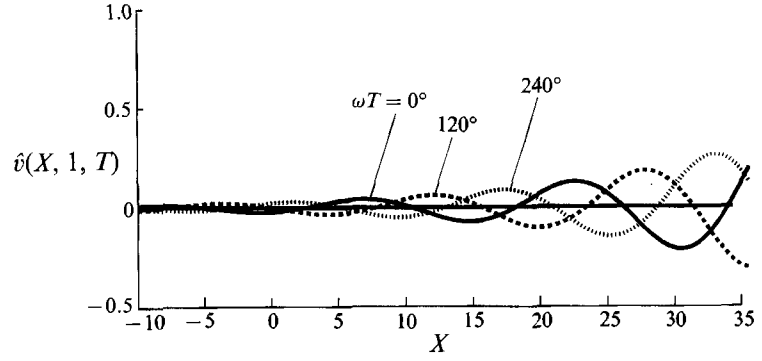

FIGURE 3. Cross-stream velocity component due to instability mode only, for three values of time: $U_1 = 1, U_2 = 0.5, \omega = 0.3, a_1/a_2 = 0, Y_0 = 0$.

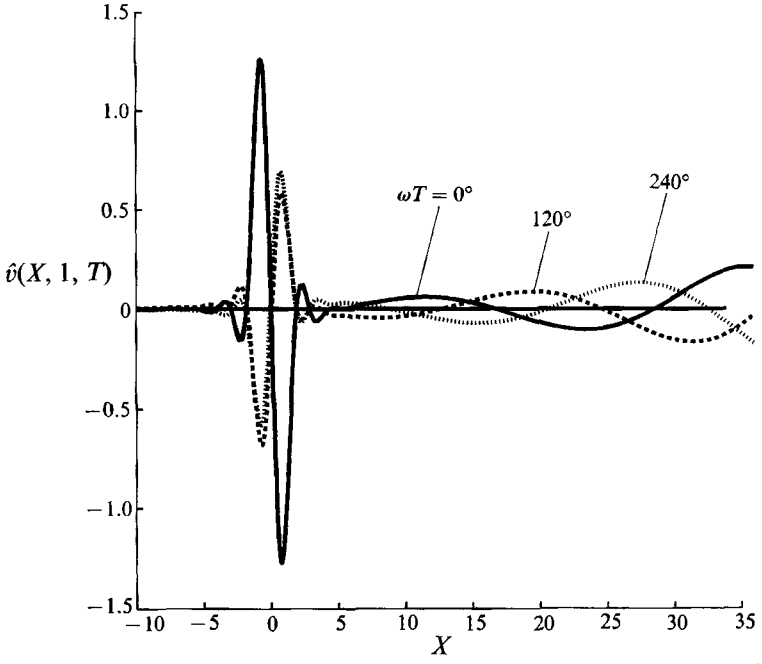

FIGURE 4. Cross-stream velocity component at upper edge of mixing layer, for three values of time: $U_1 = 1, U_2 = 0.5, \omega = 0.2, a_1/a_2 = 0, Y_0 = 0$.

examples, if the location of the cylinder is changed to $Y_0 = -0.5$, the peak of the local field is still about 0.35 and the placement of the cylinder at the lower edge of the mixing layer (i.e. at $Y_0 = -1$) reduces the peak to about 0.12 (which is still comparable to the magnitude of the instability mode within one wavelength behind the cylinder).

When the cross-stream velocity component is evaluated approximately using only the contribution from the unstable pole (37), the results are as shown in figure 3. As expected, the true hydrodynamic and local fields are absent, and for $X > X_\infty$ ($X_\infty \approx$ 7–10), the visual agreement with the corresponding curves in figure 2 is complete. This suggests that in order to observe accurately the instability wave, the point of observation should be at least 4–5 vorticity thicknesses behind the cylinder. This requirement becomes more severe as $(Y - Y_0)$ is reduced because of the contamination

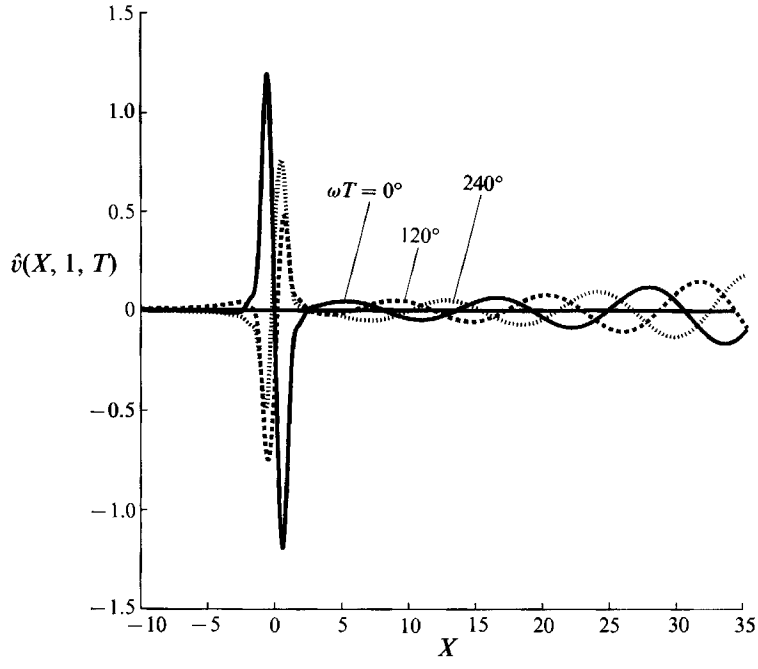

FIGURE 5. Cross-stream velocity component at upper edge of mixing layer, for three values of time: $U_1 = 1, U_2 = 0.5, \omega = 0.4, a_1/a_2 = 0, Y_0 = 0$.

by the large local field. Putting it differently, we feel that the observation point should be at least $\frac{3}{4}$ of a wavelength downstream of the cylinder in order to detect the instability wave with confidence; at the other extreme, observations taken within 1–2 vorticity thicknesses of the cylinder cannot possibly reflect the true nature of this wave. Note that the relevant scaling parameter for the appearance of the instability wave behind the cylinder is the characteristic thickness of the mixing layer and not the characteristic size of the body. These remarks qualitatively apply to cases in which the excitation frequency is (roughly) the same as the most unstable frequency (which is true for figures 2 and 3).

For the cases when the excitation frequency is shifted to either side of the most unstable frequency, the results are as presented in figures 4 and 5. These are very similar to figure 2. When the frequency is reduced (figure 4), there is more detail in the local field because the relevant lengthscale (the wavelength) has increased and the decay of the hydrodynamic field is slower. Note that in classical potential theory, multipoles of a given order decay at the same rate with distance from the source. However, they do not decay at identical rates as $|X| \to \infty$ and Y fixed. This is easy enough to see from Appendix C. In a shear flow the situation is more complicated because the decay with X becomes frequency dependent. For example, a $(1, 1)$ quadrupole decays as $-\mathrm{i}\omega U_0'/(\mathrm{i}\omega X)^2$ as $|X| \to \infty$. We omit the details for brevity.

The appearance of a large local field is related to the presence of quadrupoles and octopoles, and their behaviour as R^{-2} and R^{-3} in the overlap region. In other words, R does not need to become a great deal smaller than unity before R^{-3} becomes quite large. The outer field consists of disturbances generated by the actual multipoles and their images in the interfaces at $Y = \pm 1$. The nearest images are at $Y = 2 - Y_0$ and at $-Y = 2 + Y_0$ (see (B 4)). These images are highly non-standard: for example, when ω and ΔU are small, a quadrupole at Y_0 induces dipoles at the nearest image points.

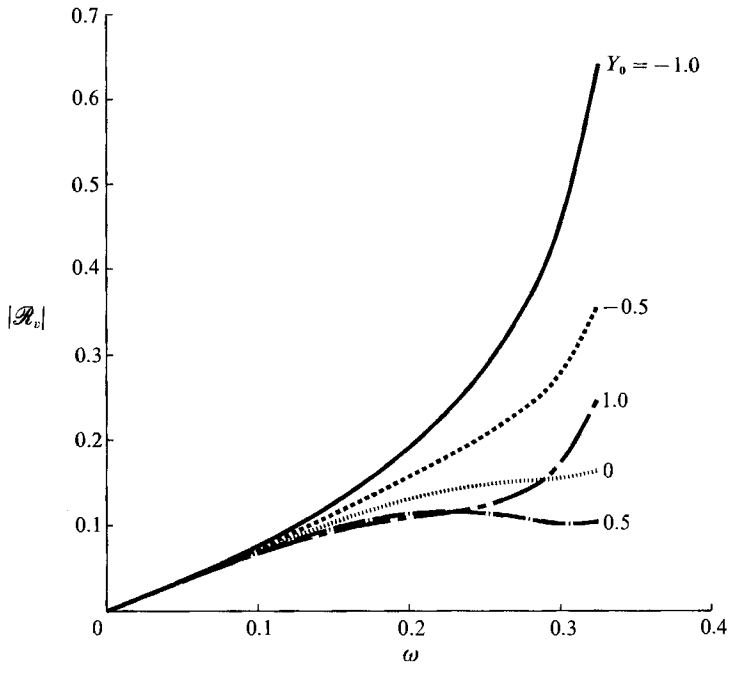

FIGURE 6. v-receptivity as a function of frequency for parameter values of cylinder location: $U_1 = 1, U_2 = 0.2, a_1/a_2 = 0$.

We were not entirely successful in fully understanding the image structure of the flow field for arbitrary values of these parameters (see Lighthill 1958).

It is also interesting to note from the previous figures that the hydrodynamic field behind the cylinder decays to very small values (almost zero) before the instability wave forces the disturbance to grow behind the cylinder. This phenomenon is also present in leading-edge receptivity, although the physical mechanism is quite different owing to the streamwise decay of the Lam–Rott eigenfunctions (Goldstein & Hultgren 1989).

A representative result for the v-receptivity is shown in figure 6 as a function of frequency, ω, for parametric values of the cylinder position Y_0. Quite generally, this receptivity increases with excitation frequency, although we believe that the rather rapid increase at the highest frequencies (above about 0.3) may be questionable because of the unphysical stability behaviour of the Rayleigh velocity profile in the neighbourhood of the neutral wavenumber (or neutral frequency = 0.3835), owing to a square root (rather than linear) dependence of growth rate on $(k-k_N)$. At low frequencies, receptivity is proportional to frequency and is insensitive to cylinder position. Both of these observations make sense physically because, in the long-wave limit, streamwise variations are gentle, therefore, the cross-stream velocity component must be small according to continuity. Furthermore, in this same limit, an $O(1)$ change in Y_0 is negligible on the scale of the wavelength. It is also seen that the mixing layer is most receptive to excitation at the low-speed edge ($Y_0 = -1$) and least receptive to that at the high-speed side ($Y_0 = 1$); this behaviour is not completely monotonic, however. The previous remarks apply to many other sets of parameters for which we cannot present the data because of space limitations. Our results are also consistent with those in Balsa (1988).

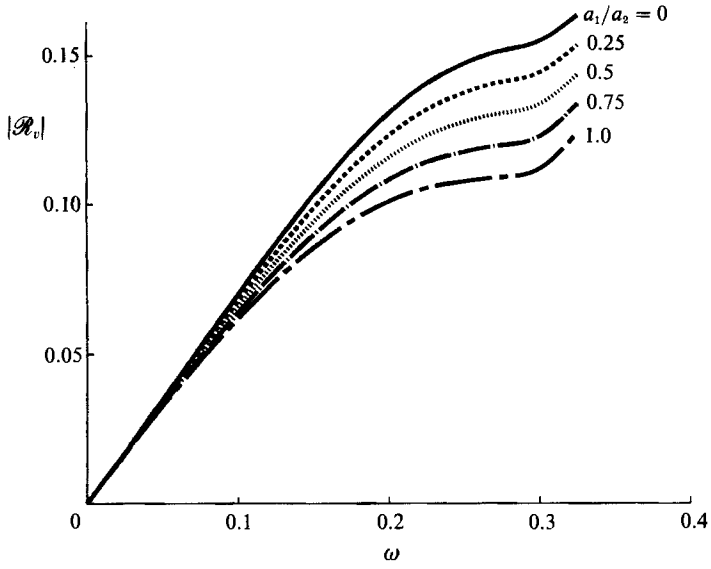

FIGURE 7. v-receptivity as a function of frequency for parameter values of amplitude ratio: $U_1 = 1, U_2 = 0.2, Y_0 = 0, \phi = 0$.

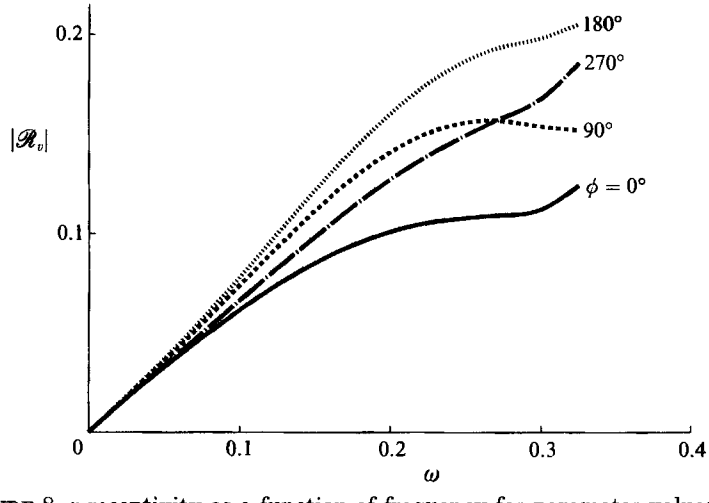

FIGURE 8. v-receptivity as a function of frequency for parameter values of phase: $U_1 = 1, U_2 = 0.2, a_1/a_2 = 1, Y_0 = 0$.

The results in figure 7 indicate the behaviour of v-receptivity for parametric values of $(a_1/a_2) \leqslant 1$. As the cylinder is made to oscillate simultaneously in the streamwise and cross-stream directions, the receptivity decreases by about 30% at the higher frequencies. However, the receptivity at any amplitude ratio, a_1/a_2, may be changed by as much as a factor of 2 by varying the phase relationship between the X- and Y-motions. Representative results are presented in figure 8. We believe that if the orbital motion of the cylinder is such that it tends to follow the velocity fluctuations associated with the instability wave in the mixing layer, receptivity will be enhanced.

The v-receptivity of a mixing layer may be reduced sharply by reducing the velocity ratio $\Delta U/2U_m$. This has been observed previously by the author (Balsa

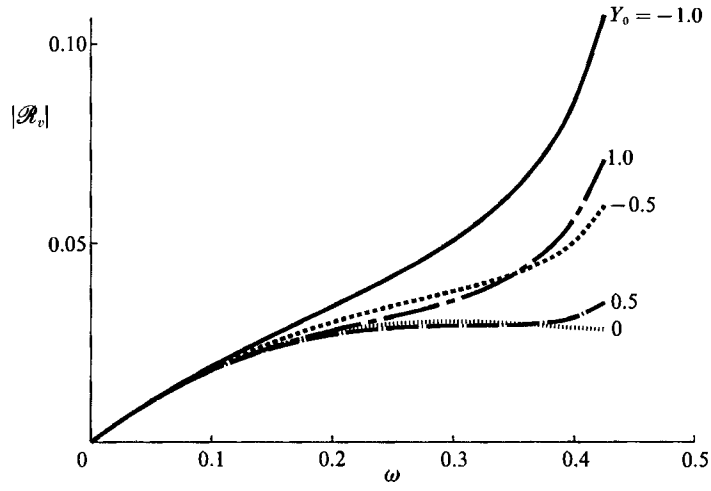

FIGURE 9. v-receptivity as a function of frequency for parameter values of cylinder location: $U_1 = 1, U_2 = 0.5, a_1/a_2 = 0$.

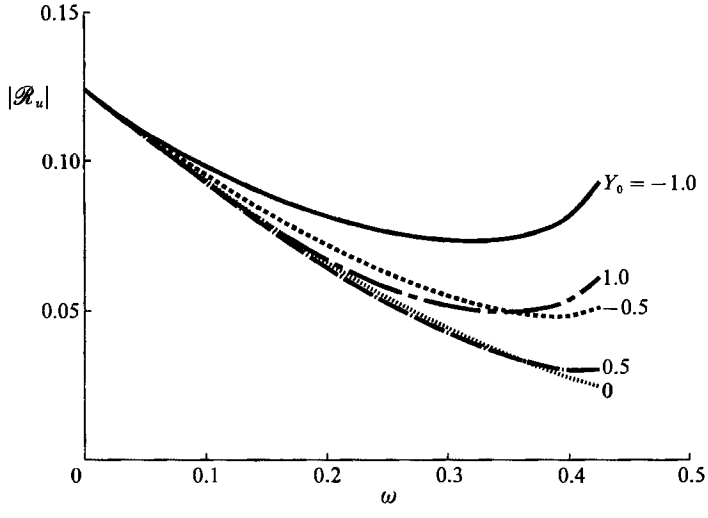

FIGURE 10. u-receptivity as a function of frequency for parameter values of cylinder location: $U_1 = 1, U_2 = 0.5, a_1/a_2 = 0$.

1988). One such result is shown in figure 9; when compared with figure 6, it is seen that at intermediate frequencies, receptivity is reduced by a factor of 5–8. Finally, figure 10 shows the behaviour of u-receptivity for parametric values of Y_0; it is to be compared to figure 9 for the corresponding v-receptivity. Note that u-receptivity is maximum at $\omega = 0$. Our results indicate that in the vicinity of the most unstable frequency ($\omega \approx 0.3$), both receptivities are relatively large, but neither is at its maximum.

To conclude, the complete velocity field exhibits a rather complex behaviour as a function of the streamwise coordinate. Near the axial position of the cylinder, the flow is dominated by a strong local field, and the instability wave does not emerge dominantly until about $\frac{3}{4}$ wavelength (4–5 vorticity thicknesses) behind the cylinder. This fact should be kept in mind by experimentalists who, in the author's opinion,

often make some of their measurements on instability waves too close to the body. Receptivities for the u- and v-velocities behave very differently as functions of excitation frequency. The velocity ratio has an important effect on these receptivities; receptivity decreases with velocity ratio.

I wish to thank my colleague Dr E. J. Kerschen for numerous discussions on this problem and for bringing Lighthill's paper to my attention. Conversations with Professor M. Gaster were also very helpful. The continued financial support by NASA Lewis Research Center and by the Institute for Computational Mechanics in Propulsion (ICOMP) on various aspects of hydrodynamic instability is gratefully acknowledged. This paper is dedicated to the memory of my father, who died on January 10, 1992.

Appendix A. Steady solutions

The main purpose of this appendix is to document the steady solutions, $(\cdot)_s$, without any derivation. At $O(\epsilon)$ we have

$$\boldsymbol{v}_s^{(1)} = (u_s^{(1)}, v_s^{(1)}) = -(U_0'/2r^3)(\sin 3\theta, -\cos 3\theta) \tag{A 1}$$

and

$$-P_s^{(1)} = -p_s^{(1)} = U_0 u_s^{(1)} + \boldsymbol{v}^{(0)} \cdot \boldsymbol{v}_s^{(1)} + U_0' u^{(0)} r \sin\theta + U_0' U_0 (\sin\theta)/r. \tag{A 2}$$

U_0 and U_0' denote U and $\mathrm{d}U/\mathrm{d}Y$ evaluated at Y_0. The integral of (A 2) around the cylinder immediately yields the steady force, (13a). Note that $\boldsymbol{v}^{(0)} = (u^{(0)}, v^{(0)})$ is given by (8a).

At $O(\epsilon^2)$, the situation is more complicated since the steady flow is no longer irrotational. Let $\zeta_s^{(2)}$ denote the spanwise component of the perturbation vorticity at this order; it satisfies

$$\left(U_0 \frac{\partial}{\partial \xi} + \boldsymbol{v}^{(0)} \cdot \frac{\partial}{\partial \boldsymbol{\xi}}\right) \zeta_s^{(2)} = U_0'' v^{(0)}. \tag{A 3}$$

Thus, this vorticity disturbance arises from the vertical displacement of a material volume in the non-uniform base flow. The solution of (A 3), which vanishes at $r = \infty$, is

$$\zeta_s^{(2)} = U_0'' \sin\theta / r \tag{A 4}$$

and the corresponding velocity components which satisfy the correct boundary conditions on the cylinder surface are

$$u_s^{(2)} = -\tfrac{1}{2} U_0''(\log r + \sin^2\theta) - (U_0''/8r^2)(\cos 2\theta - (\cos 4\theta)/r^2), \tag{A 5}$$

$$v_s^{(2)} = \tfrac{1}{4} U_0''(\sin 2\theta - (\sin 2\theta)/2r^2 + (\sin 4\theta)/2r^4). \tag{A 6}$$

The expression for the steady pressure at this order is not needed.

Note the very important fact that the $O(r^{-2})$ term in $\boldsymbol{v}_s^{(2)} = (u_s^{(2)}, v_s^{(2)})$ will actually produce an unsteady term at $O(\epsilon^3)$ (i.e. at lowest order) in the outer field. This is how vorticity fluctuations are imparted to the outer flow by the oscillating cylinder. The outer (rotational) field is also capable of converting a purely irrotational inner field (such as $\boldsymbol{v}^{(0)}$) into a vortical disturbance, as shown in the main body of this paper, (28). Observe that the form of (A 3) is reminiscent of the Rayleigh equation. Note also that at higher orders it is not possible to require the perturbation velocity components to decay as $r \to \infty$; their behaviour at large r is actually determined by the asymptotic matching. Thus, for example, $u_s^{(2)} \sim \log r$.

Appendix B. Green's function for a piecewise linear profile

The piecewise linear velocity profile of Rayleigh is shown in figure 11. This profile has been used in other studies (Balsa 1987) where its relationship to infinitely differentiable profiles and viscous flows is discussed within the context of linear stability theory. Suffice it here to remark that this profile yields extremely realistic stability results provided that the frequency of excitation is not in the immediate vicinity of the neutral frequency.

The specific form of this profile is

$$U(Y) = \begin{cases} U_1 = \text{const.}, & Y \geqslant +1, \\ U_m(1+\gamma Y), & |Y| < 1, \\ U_2 = \text{const.}, & Y \leqslant -1, \end{cases} \tag{B 1}$$

where $U_m = \frac{1}{2}(U_1+U_2)$ and $\gamma = \Delta U/2U_m$ with $\Delta U = U_1 - U_2 > 0$. It is customary to call γ the velocity ratio. The usefulness of this profile lies in the fact that the vorticity associated with it is (sectionally) constant so that the perturbed flow is essentially irrotational. For this reason, it is a simple matter to obtain this flow.

As customary, across the mean positions of the material interfaces at $Y = \pm 1$, we require the continuity of pressure and fluid particle displacement. In each of the regions A, B, C, and D of figure 11 we write the solutions to the homogeneous version of (19) as a linear combination of $\exp(\pm \kappa Y)$ where κ is defined by (20). After some straightforward algebra, we obtain for these solutions

$$\mathscr{G}_1(k, Y, \omega) = \begin{cases} \exp[-\kappa(Y-1)] & \text{in region A,} \quad (\text{B } 2a) \\ \exp[-\kappa(Y-1)] + \dfrac{\Delta U}{2\kappa}\dfrac{k}{\omega_1}\sinh[\kappa(Y-1)] & \text{in region B,} \quad (\text{B } 2b) \end{cases}$$

$$\mathscr{G}_2(k, Y, \omega) = \begin{cases} \exp[\kappa(Y+1)] + \dfrac{\Delta U}{2\kappa}\dfrac{k}{\omega_2}\sinh[\kappa(Y+1)] & \text{in region C,} \quad (\text{B } 2c) \\ \exp[\kappa(Y+1)] & \text{in region D,} \quad (\text{B } 2d) \end{cases}$$

where

$$\omega_j = \omega + kU_j, \quad j = 1, 2 \tag{B 2e}$$

and k is the transform variable. The solution above assumes that the source point is within the mixing layer proper; we believe this is the most interesting case (i.e. $|Y_0| \leqslant 1$). Note that (B 2a, b) and (B 2c, d) already satisfy the interface conditions on $Y = \pm 1$.

In order to write down Green's function, $\tilde{G}$, compactly, we need some definitions. Let

$$\Omega_{1,2}(k) = -kU_m \pm i\Delta U\lambda(k), \quad \lambda(k) = \tfrac{1}{4}[\exp(-4\kappa) - (1-2\kappa)^2]^{\frac{1}{2}}, \tag{B 3a, b}$$

where the branch points of the square root in (B 3b) are at $k = \pm k_N (k_N \approx 0.6392)$ and the branch cuts are chosen to lie along the real k-axis with $|k| > k_N$. The unstable and stable dispersion relations are given by Ω_2 and Ω_1, respectively. They should be viewed as complex-valued functions, $\omega = \Omega_{1,2}(k)$, of the complex wavenumber k.

Although the position of the source has been restricted by the inequality $|Y_0| \leqslant 1$, the observer position, Y, may take on any value. The most interesting case arises when Y is also within the mixing layer proper. In this case, after some algebra, we find in region B (i.e. $Y_0 < Y \leqslant 1$)

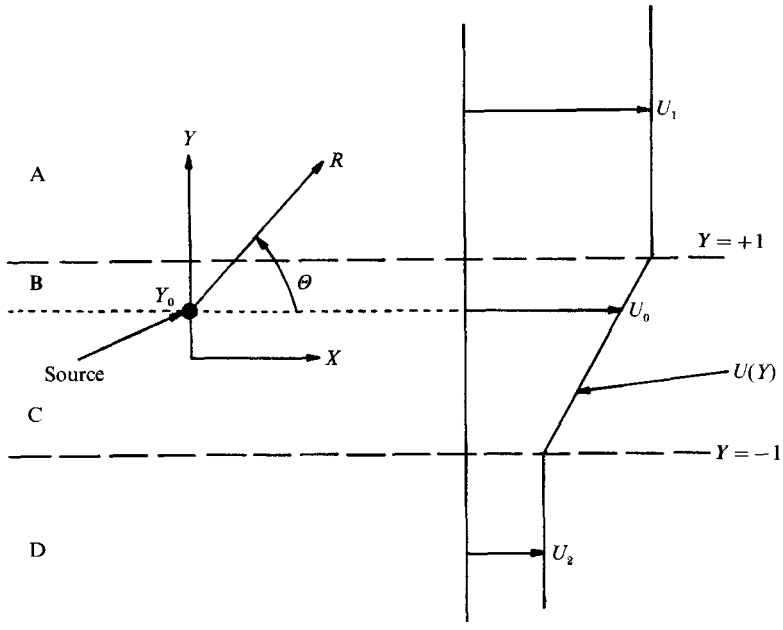

FIGURE 11. Piecewise linear velocity profile, $|Y_0| < 1$.

$$\tilde{G}(k,Y,\omega;Y_0) = -\frac{1}{2\kappa(\omega-\Omega_1)(\omega-\Omega_2)}\left\{\left[\omega_1\omega_2+\left(\frac{\Delta U}{2}\right)^2(\kappa-\tfrac{1}{4})\right]\exp[-\kappa(Y-Y_0)]\right.$$
$$+\frac{\Delta U}{4}\left(\frac{\Delta U}{4}+\frac{k\omega_2}{\kappa}\right)\exp[\kappa(Y+Y_0-2)]$$
$$+\frac{\Delta U}{4}\left(\frac{\Delta U}{4}-\frac{k\omega_1}{\kappa}\right)\exp[-\kappa(Y+Y_0+2)]$$
$$\left.-\left(\frac{\Delta U}{4}\right)^2\exp[\kappa(Y-Y_0-4)]\right\}, \tag{B 4}$$

where we have used (21*a*). If Y lies in region C, interchange Y and Y_0 in (B 4).

Essentially, $\tilde{G}$ is an analytic function of k except for a branch cut along the imaginary axis and possible simple poles at $\omega = \Omega_{1,2}(k)$ (since ω is given, the previous equation defines the values of k at these poles). The branch cuts of $\lambda(k)$ cancel when $(\omega-\Omega_1)(\omega-\Omega_2)$ is multiplied out.

Thus we have a simple explicit representation of Green's function that greatly facilitates the numerical inversion of Fourier transform (22).

Appendix C. Behaviour of multipoles near the source

If we differentiate (24*a*, *b*) with respect to the variables indicated in (17*b*), we get the following set of results as $R \to 0$:

Quadrupole

$$\exp(-i\omega T)\,G_{20} = -\frac{1}{2\pi}\frac{\cos 2\Theta}{R^2}+\frac{U_0''}{4\pi U_0}\left(\log R+\frac{\cos 2\Theta}{2}+\text{arb.}\right)+O(R), \tag{C 1a}$$

$$\exp(-i\omega T)\,G_{02} = \frac{1}{2\pi}\frac{\cos 2\Theta}{R^2}+\frac{U_0''}{4\pi U_0}\left(\log R-\frac{\cos 2\Theta}{2}+\text{arb.}\right)+O(R), \tag{C 1b}$$

$$\exp(-i\omega T)\,G_{11} = \frac{1}{2\pi}\frac{\sin 2\Theta}{R^2}-\frac{U_0''}{8\pi U_0}(\sin 2\Theta+\text{arb.})+O(R); \tag{C 1c}$$

Octopole

$$\exp(-i\omega T)\,G_{30} = \frac{1}{\pi}\frac{\cos 3\Theta}{R^3} + \frac{U_0''}{4\pi U_0 R}(\cos\Theta + \sin\Theta\sin 2\Theta) + O(1), \qquad (C\ 2a)$$

$$\exp(-i\omega T)\,G_{21} = -\frac{1}{\pi}\frac{\sin 3\Theta}{R^3} + \frac{U_0''}{4\pi U_0 R}\sin\Theta\cos 2\Theta + O(1), \qquad (C\ 2b)$$

$$\exp(-i\omega T)\,G_{12} = -\frac{1}{\pi}\frac{\cos 3\Theta}{R^3} + \frac{U_0''}{4\pi U_0 R}\cos\Theta\cos 2\Theta + O(1), \qquad (C\ 2c)$$

$$\exp(-i\omega T)\,G_{03} = \frac{1}{\pi}\frac{\sin 3\Theta}{R^3} - \frac{U_0''}{4\pi U_0 R}(\sin\Theta + \cos\Theta\sin 2\Theta) + O(1), \qquad (C\ 2d)$$

where

$$R = [X^2 + (Y - Y_0)^2]^{\frac{1}{2}}, \quad \Theta = \tan^{-1}[(Y - Y_0)/X], \qquad (C\ 3a, b)$$

and arb. denotes arbitrary (non-essential) constants, which may be different in (C 1*a–c*).

The dipole solutions (G_{10} and G_{01}) behave as R^{-1} near the source and cannot be matched to the inner solution. Note that in order to distinguish between the G_{20} and G_{02} quadrupoles, we need the higher-order terms given in (C 1*a*, *b*). These two quadrupoles are identical in classical potential theory but are quite different for Rayleigh's equation. This should not be surprising since the base flow is homogeneous in X but not in Y.

Appendix D. Causality and the exponential integral

With reference to the second term in (35*a*), consider

$$I(\omega) = \int_0^{+\infty} \frac{\exp[ikX - \kappa(Y - Y_0)]}{k - k^*(\omega)}\,dk, \quad Y > Y_0, \qquad (D\ 1)$$

where ω is complex ($-\mathrm{Im}(\omega) = -\omega_I = \alpha \gg 1$), $\kappa = k$, and k^* is a known analytic function of ω. Here, k^* stands for k_1^* or k_2^*, where these quantities are the stable and unstable spatial eigenvalues, which behave somewhat differently as a function of ω. In order to deal with both of the eigenvalues, we use the generic quantity k^* [$\mathrm{Re}(k^*) > 0$, whereas its imaginary part may be positive or negative depending on ω and whether we consider the stable or unstable eigenvalues]. We need to reinterpret integral (D 1) in such a way that $I(\omega)$ remains analytic in the strip $-\alpha \leqslant \omega_I \leqslant 0$. Thus we satisfy causality (Briggs 1964; Bers 1975).

For ω sufficiently complex $k^*(\omega)$ lies in the first quadrant for $\mathrm{Re}(\omega) < 0$. This may be seen from (B 3*a*). As the imaginary part of ω is reduced, k^* either stays in the first quadrant (stable mode) or migrates into the fourth quadrant (unstable mode). The representative motion of $(-k^*)$ is indicated by the dashed curves in figure 12.

We simplify (D 1) through a sequence of transformations. let

$$s = -iX + (Y - Y_0), \quad \mathrm{Re}(s) > 0, \qquad (D\ 2a)$$

and define two complex planes τ and σ

$$\tau = k - k^*, \quad \sigma = s\tau, \qquad (D\ 2b, c)$$

so that

$$I(\omega) = \exp(-sk^*)\int_{-sk^*}^{+\infty} \frac{\exp(-\sigma)}{\sigma}\,d\sigma. \qquad (D\ 2d)$$

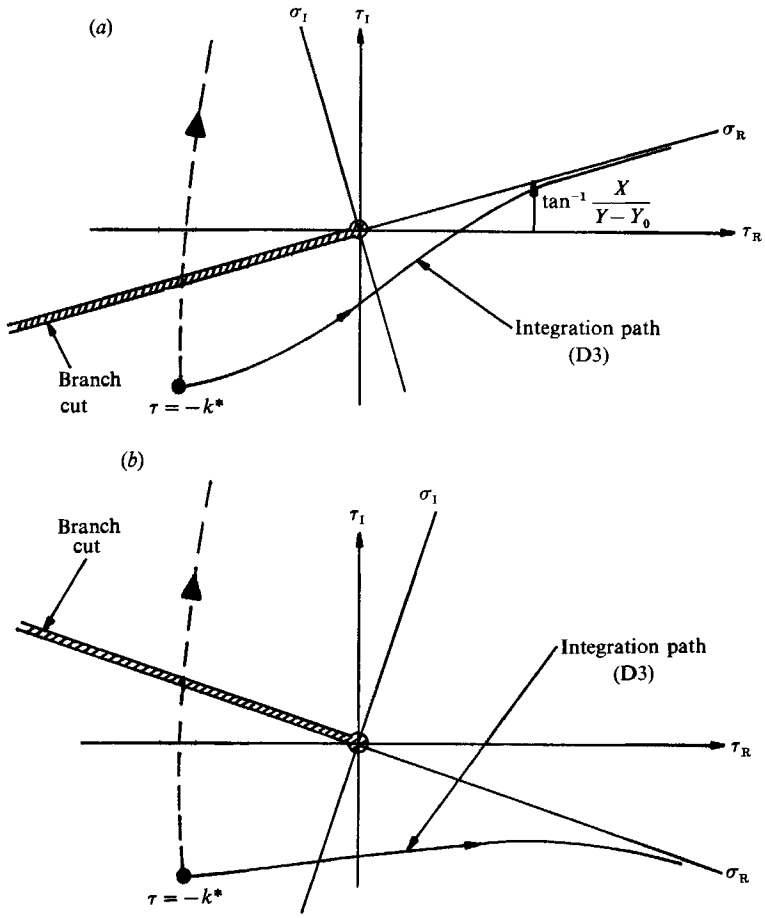

FIGURE 12. Geometry of complex τ- and σ-planes for exponential integral, $(Y-Y_0)>0$: (*a*) $X>0$, (*b*) $X<0$. The dashed curve indicates a typical path of $(-k^*)$ as $\mathrm{Im}(\omega)$ is reduced to zero.

The geometry of these complex planes is shown in figure 12. Causality can be enforced by a suitable choice for the contour of integration in (D 2*d*), which is generally dependent on (sk^*). This is a restatement of the original idea of Briggs (1964), who restricts his discussion to the much more complicated Fourier inverse (22), without separating out the kernel of the problem.

Here, we offer an entirely new and strikingly simple approach to causality: fix the path of integration in (D 2*d*) in such a way that the integral becomes a known function whose properties have been studied extensively. To achieve this, always integrate (D 2*d*) along a path that excludes the origin and does not cross the negative (real) σ-axis. Then

$$\oint_{-sk^*}^{+\infty}\frac{\exp(-\sigma)}{\sigma}\mathrm{d}\sigma = E_1(-sk^*), \tag{D 3}$$

where $E_1(z)$ is the exponential integral

$$E_1(z) = \oint_z^{+\infty}\frac{\exp(-\sigma)}{\sigma}\mathrm{d}\sigma, \quad |\arg(z)|<\pi \tag{D 4}$$

(whose properties are known; Abramowitz & Stegun 1970, p. 228). We use $\oint$ to denote this special path. Indeed, for ω sufficiently complex, this is the correct value of the *causal* integral since $\tau = -k^*$ is far down in the third quadrant of the τ-plane and it is permissible to integrate (D 2*d*) parallel to the τ_R-axis (essentially along k_R-axis). A minor contour deformation and closure at infinity immediately yield (D 3).

Now recall that $E_1(z)$ possesses a log-type branch point at $z = 0$ and a branch cut that is conventionally chosen to lie along the negative (real) z-axis.

Suppose the imaginary part of ω is reduced to zero. Then $(-k^*)$ will migrate from the third quadrant toward (into) the second quadrant of the τ-plane and the possibility exists that the branch cuts of E_1, shown in figure 12, are crossed. Whether this will actually happen or not depends on X, $Y-Y_0$, and whether k^* is k_1^* or k_2^*. If it does not happen

$$I(\omega) = \exp(-sk^*)\,E_1(-sk^*), \tag{D 5a}$$

and if it does happen

$$I(\omega) = \exp(-sk^*)\{E_1(-sk^*)+2\pi\mathrm{i}\}. \tag{D 5b}$$

The addition of $(2\pi\mathrm{i})$ in (D 5*b*) ensures that the value of $I(\omega)$ does not change as the branch cut is crossed (although the value of E_1 does). Thus, the analyticity of $I(\omega)$ is preserved.

The previous results are universal. Essentially, causality is expressed by choosing the proper branch for an exponential-like integral. We also mention that the translation of these ideas into a FORTRAN computer code is very simple through a systematic use of subroutines.

We can easily verify the validity of the above results in the far field. Note the asymptotic expansion

$$E_1(z) = \frac{\exp(-z)}{z}\left(1-\frac{1}{z}+\ldots\right), \quad |\arg(z)| < \frac{3\pi}{2}, \tag{D 6}$$

and let $X \gg 1$ (far downstream). With reference to figure 12(*a*), the angle of inclination between the σ_R- and τ_R-axes is large (near $\frac{1}{2}\pi$) so that both the unstable and stable eigenvalues will migrate across the branch cut. Thus (D 5*b*) becomes

$$I(\omega) \sim 2\pi\mathrm{i}\exp(-sk^*) - 1/sk^* + \ldots, \tag{D 7a}$$

which is exponentially growing (decaying) in X depending on whether k_1^* is negative (positive). Thus both the unstable and stable modes are found on the downstream side. This clearly indicates that the instability is excited by the source and is convected downstream.

Next, let $(-X) \gg 1$ (far upstream). With reference to figure 12(*b*), neither the unstable nor the stable eigenvalues will migrate across the branch cut. Thus, (D 5*a*) becomes

$$I(\omega) \sim -1/sk^* + \ldots \tag{D 7b}$$

and no instability modes are found on the upstream side.

It is important to remember that we are looking at convectively unstable flows. This concept is somewhat hidden in our assumption that the eigenvalues k_1^* and k_2^* are distinct for any (complex) ω in a certain strip. Thus, the poles of (22) are always simple; this ultimately leads to the presence and importance of the exponential integral. In other words, our analysis clearly fails if $\Omega_1'(k_1^*) = 0$, etc. (see (35*a*)) for some value of ω with $\mathrm{Im}(\omega) \leqslant 0$. In this case, the flow is absolutely unstable (Huerre & Monkewitz 1985).

REFERENCES

ABRAMOWITZ, M. & STEGUN, I. A. 1970 *Handbook of Mathematical Functions*. Dover.

BALSA, T. F. 1987 On the spatial instability of piecewise linear free shear layers. *J. Fluid Mech.* **174**, 553–563.

BALSA, T. F. 1988 On the receptivity of free shear layers to two-dimensional external excitation. *J. Fluid Mech.* **187**, 155–177.

BATCHELOR, G. 1967 *An Introduction to Fluid Dynamics*. Cambridge University Press.

BERS, A. 1975 Linear waves and instabilities. In *Plasma Physics* (ed. C. DeWitt & J. Peyraud). Gordon and Breach.

BETCHOV, R. & CRIMINALE, W. O. 1967 *Stability of Parallel Flows*. Academic.

BRIGGS, R. J. 1964 *Electron-Stream Interaction with Plasmas*. MIT Press.

CHANDRASEKHAR, S. 1961 *Hydrodynamic and Hydromagnetic Stability*. Oxford University Press.

DRAZIN, P. G. & REID, W. H. 1981 *Hydrodynamic Stability*. Cambridge University Press.

GOLDSTEIN, M. E. 1983 The evolution of Tollmien–Schlichting waves near a leading edge. *J. Fluid Mech.* **127**, 59–81.

GOLDSTEIN, M. E. 1985 Scattering of acoustic waves into Tollmien–Schlichting waves by small streamwise variations in surface geometry. *J. Fluid Mech.* **154**, 509–530.

GOLDSTEIN, M. E. & HULTGREN, L. 1989 Boundary-layer receptivity to long-wave free-stream disturbances. *Ann. Rev. Fluid Mech.* **21**, 137–166.

HEINRICH, R. A., CHOUDHARI, M. & KERSCHEN, E. J. 1988 A comparison of boundary layer receptivity mechanisms. Presented at *First Natl Fluid Dynamics Conf. Cincinnati*.

HUERRE, P. & MONKEWITZ, P. 1985 Absolute and convective instabilities in free shear layers. *J. Fluid Mech.* **159**, 151–168.

HUERRE, P. & MONKEWITZ, P. A. 1990 Local and global instabilities in spatially developing flows. *Ann. Rev. Fluid Mech.* **22**, 473–537.

LIGHTHILL, M. J. 1958 The fundamental solution for small steady three-dimensional disturbances to a two-dimensional parallel shear flow. *J. Fluid Mech.* **3**, 113–144.

SCHUBAUER, G. B. & SKRAMSTAD, H. K. 1943 Laminar boundary-layer oscillations and transition on a flat plate. *Natl Bur. Stand. Res. Paper* 1772.

TAYLOR, G. I. 1917 Motion of solids in fluids when the flow is not irrotational. *Proc. R. Soc. Lond.* A **93**, 99–113.

VAN DYKE, M. 1975 *Perturbation Methods in Fluid Mechanics*. Parabolic.